Accounting for taste: A multi-attribute neurocomputational model explains the neural dynamics of choices for self and others

Alison Harris*[†1], John A. Clithero[2], Cendri A. Hutcherson[3,4]

[1]Department of Psychology, Claremont McKenna College, Claremont, CA USA
[2]Department of Economics, Pomona College, Claremont, CA USA
[3]Department of Psychology, University of Toronto Scarborough, Toronto, ON Canada
[4]Department of Marketing, Rotman School of Management, Toronto, ON Canada

ABBREVIATED TITLE: A neurocomputational model of choices for others

Address correspondence to:
Alison Harris, PhD
Department of Psychology
Claremont McKenna College
850 Columbia Avenue
Claremont, CA 91711
aharris@cmc.edu

[†]All authors contributed equally to the work.

Number of pages: 47
Number of figures/tables: 7/2
Number of words for Abstract/Introduction/Discussion: 250/646/1496
Conflict of interest: The authors declare no competing financial interests.

Abstract

How do we make choices for others with different preferences from our own? Although neuroimaging studies implicate similar circuits in representing preferences for oneself and others, some models propose that additional corrective mechanisms come online when choices for others diverge from one's own preferences. Here we exploited the high temporal resolution of event-related potentials (ERP), in combination with computational modeling, to examine how social information is integrated in the time leading up to choices for oneself and others. Hungry participants with unrestricted diets selected foods for themselves, a similar unrestricted eater, and a dissimilar, self-identified healthy eater. Across choices for both oneself and others, ERP value signals emerged within the same time window but differentially reflected taste and health attributes based on the recipient's preferences. Choices for the dissimilar recipient were associated with earlier activity localized to brain regions implicated in social cognition including temporoparietal junction (TPJ). Finally, response-locked analysis revealed a late ERP component specific to choices for the similar recipient, localized to the parietal lobe, that appeared to reflect differences in the response threshold based on uncertainty. A multi-attribute computational model supported the link between specific ERP components and distinct model parameters, and was not significantly improved by adding time-dependent dual processes. Model simulations suggested that longer response times (RTs) previously associated with effortful correction may alternatively arise from higher choice uncertainty. Together these results provide a parsimonious neurocomputational mechanism for social decision-making, additionally explaining divergent patterns of choice and RT data in decisions for oneself and others.

Significance Statement

How do we choose for others, particularly when they have different preferences? Whereas some studies suggest that similar neural circuits underlie decision-making for oneself and others, others argue for additional, slower perspective-taking mechanisms. Combining event-related potentials with computational modeling, we found that integration of others' preferences occurs over the same timescale as for oneself, while differentially tracking recipient-relevant attributes. Although choosing for others took longer and produced differences in late-emerging neural responses, computational modeling attributed these patterns to greater response caution rather than egocentric bias correction. Computational simulations also correctly predicted when and why choosing differently for others takes longer, suggesting that a model incorporating value integration and evidence accumulation can parsimoniously account for complex patterns in social decision-making.

Whether in parenting or politics, we are often required to make decisions for other individuals whose preferences may differ substantially from our own. A critical question concerns whether and when such choices require perspective-taking mechanisms that are slower, more effortful, or computationally costly (Epley et al., 2004). For example, studies of response time (RT) find that people take longer to choose for similar others when those choices diverge from what they choose for themselves (Tamir and Mitchell, 2013; Apps et al., 2016; Volz et al., 2017), perhaps because slower, more controlled processing is required to adjust an otherwise automatic egocentric bias. Overcoming egocentric choice biases has also been associated with increased activation in brain regions associated with social cognition, such as the ventromedial prefrontal cortex (VMPFC) and temporoparietal junction (TPJ) (Tamir and Mitchell, 2010; Silani et al., 2013).

Yet recent work using computational modeling suggests that slower RTs and activation in VMPFC and TPJ during some social decision-making tasks can result from a noisy value-integration mechanism, without requiring additional slow or effortful cognitive processes (Hutcherson et al., 2015; Krajbich et al., 2015; Berkman et al., 2017). Moreover, several functional magnetic resonance imaging (fMRI) studies have found that constructing values and choices for oneself and others recruit the same regions of VMPFC, even when preferences differ substantially (Nicolle et al., 2012; Janowski et al., 2013). Unfortunately, the low temporal resolution of fMRI obscures the dynamics of this process, and recent computational models of choice for others (Devaine and Daunizeau, 2017; Tarantola et al., 2017) have not explicitly examined when and why constructing values for others might require longer, more extensive processing compared to the self.

This paper aims to answer three related questions. First, are additional neural computations involved when choosing for others with similar or dissimilar preferences? Second, what are the temporal dynamics of those computations? Third, how might these computations explain when and why people show egocentric biases, or instead make different choices for themselves and others? To address these questions, we use a dietary choice task (Figure 1) in which participants with unrestricted diets made food choices for themselves and two partners: a *Similar* partner with unrestricted dietary preferences, and a *Dissimilar* partner who self-identified as a healthy eater. We employed a novel combination of event-related potentials (ERP), computational modeling, and simulation to identify the processes necessary to account for the full pattern of choices, RTs, and neural responses observed when choosing for oneself, similar, and dissimilar others.

The best-fitting model, a multi-attribute version of the drift-diffusion model (DDM) (Smith and Ratcliff, 2004; Ratcliff and McKoon, 2008), suggests that individuals may indeed use their own preferences as a source of information, particularly when deciding for similar others. Yet a slow, serial adjustment mechanism is not required to explain when and why people choose differently for others and take longer to do so. Instead, an early-acting perspective-taking mechanism, localized to the temporoparietal junction (TPJ), may play a role in adjusting the importance of different stimulus attributes (e.g., tastiness and healthiness) based on inferences about the recipient's preferences. These attributes are integrated into a noisy overall value signal, localized to a region of VMPFC previously implicated in value construction (Bartra et al., 2013; Clithero and Rangel, 2014) with a similar time course regardless of recipient. We find further evidence that these VMPFC value signals serve as input to an evidence accumulation process (Rangel and Clithero, 2013) that produces a choice when the accumulated evidence crosses a

threshold whose height can be adjusted based on uncertainty about others' preferences. Thus, although choices for other involve multiple distinct systems, these computations follow different temporal dynamics and play different functional roles than previously hypothesized. These results show that a parsimonious neurocomputational framework can account not only for when people choose differently for themselves than for others, but also when and why these choices are associated with additional processing time.

Methods

Participants

Thirty-eight right-handed participants (ages 18-40, 20 female) from the Claremont Colleges participated in exchange for course credit. Participants were screened to ensure that they enjoyed common appetitive snacks and did not self-identify as healthy eaters. Although all 38 participants were included in the behavioral model, two individuals were excluded from the combined behavioral-neurophysiological model due to excessively noisy EEG data in which cognitive signals could not be reliably separated from artefactual noise using artifact removal protocols (see "EEG data acquisition and preprocessing"). All participants provided written informed consent before participation. Procedures were reviewed and approved by the Claremont McKenna College Institutional Review Board.

Stimuli

Stimuli consisted of color pictures of 250 common appetitive foods on a black background (Figure 1C; 576 x 432 pixels). Foods were chosen to span a full range of perceived tastiness and

healthiness based on pilot ratings from a separate group of participants (N = 25). The stimulus set included fruits and vegetables, chips, and candy bars.

Procedure

The experiment consisted of three parts (Figure 1A). In Part 1, participants received information about the two partners for whom they would be making food choices, after which they rated foods in terms of taste and health attributes. In Part 2, participants made choices about whether to eat these foods, separately for themselves and their two partners (*Own* self, *Similar* other, *Dissimilar* other conditions), while their brain activity was recorded with electroencephalography (EEG). Finally, in Part 3, a single trial was randomly selected for each recipient and the outcome of that trial was implemented.

Participants were instructed to fast for four hours prior to arrival to ensure they were hungry and motivated to perform the decision task. Compliance was assessed verbally before starting the experiment. Next, the experimenter took a photo of the participant against a white wall, which was employed as a visual cue for the trials in which the participant chose food for him/herself in Part 2. Participants then completed a short computer-based survey in which they indicated the extent to which they generally use health information in deciding what to eat, and made a series of twelve binary choices between a healthier and less healthy but tastier option (e.g., green salad vs. French fries).

Participants received instructions familiarizing them with the overall structure of the decision task and introducing the two partners (Figure 1B), matched to the participant's own gender. Participants were informed that the partners were real people expressing their true

151 dietary preferences, and that they had in fact agreed to eat at least three bites of whichever food
152 the participant selected for them. This was true; no deception was used in the experiment. Each
153 participant received information that one partner had unrestricted dietary preferences similar to
154 their own (*Similar* partner; Figure 1B, top), while the other had quite different preferences
155 (*Dissimilar* partner; Figure 1B, bottom). First, participants viewed two short video interviews in
156 which each partner responded to prompts about their eating habits. Each partner was introduced
157 by name via an intertitle at the beginning of the interview. During the interview, partners
158 described their food preferences in general, and answered questions about specific choices (e.g.,
159 "Pizza or a salad"). Representative quotes for the partner without dietary restrictions included:
160 "I would say for me, taste is my number one consideration when I'm eating…If it tastes good but
161 it's not healthy, I'll just eat less of it, but for me eating food is all about it tasting good."
162 Representative quotes for the self-identified healthy eater included the following: "I don't eat
163 anything with added sugars…I try to eat a lot of fruits and vegetables, and I eat a lot of peanut
164 butter and almond butter." The video interviews were lightly edited for conciseness, but
165 otherwise were not manipulated. To give participants a fuller picture of the partners' preferences,
166 they were also shown the partners' responses to the same 12-item food questionnaire they had
167 completed earlier.

168 Following introduction to the partners, participants completed two blocks of trials in
169 which they rated each of 250 appetitive foods in terms of tastiness and healthiness. Each food
170 was displayed until the participant entered a keypress response using a 4-point scale (1 = Strong
171 No, 2 = Weak No, 3 = Weak Yes, 4 = Strong Yes). The order of the rating blocks and the left-to-
172 right order of the response keys was counterbalanced across participants.

173 Next, EEG data were recorded while participants performed a simple decision-making
174 task (Figure 1C) in which they chose whether or not a particular recipient (*Own* self, *Similar*
175 other, or *Dissimilar* other) would have the opportunity to consume each food at the end of the
176 experiment. Due to time constraints, this decision task used a subset of 200 foods (out of the
177 original 250), chosen to span the full range of the participant's taste and health ratings.
178 Participants made decisions regarding each food both for themselves and the two partners,
179 resulting in a total of 600 trials, in blocks of 10 trials per recipient. At the beginning of each
180 block, the participant saw a prompt ("For the next set of trials, please choose for this person")
181 above a picture of the intended recipient. For *Own* self trials, this picture was the head shot taken
182 upon the participant's arrival at the lab; the other partners' images were captured from
183 screenshots of the video interviews. The duration of the recipient prompt was randomly jittered
184 between 4 and 5 seconds. In addition, a smaller picture of the intended recipient was displayed at
185 the top of the screen throughout the block. On each trial, participants saw a food image centered
186 on the screen, which remained visible until a response was entered (maximum duration 4 s),
187 using a 4-point scale (1 = Strong No, 2 = Weak No, 3 = Weak Yes, 4 = Strong Yes). This
188 response method captures both the strength and direction of participants' preferences (Hare et al.,
189 2009; Hutcherson et al., 2015). The order of the recipient blocks and of the food images was
190 randomized across participants. The task was subdivided into 6 runs, and within each run the
191 blocks of trials were further subdivided by intervening self-paced breaks. During the decision
192 trials, participants were instructed to maintain central fixation and minimize eye movements and
193 blinks; adherence was monitored by checking the EEG signal for stereotypical patterns of eye-
194 movement-related artifact in frontal electrodes during the recording. Following each trial, a
195 screen consisting of a fixation dot was shown for a randomly jittered inter-trial interval of 4-6

seconds. Participants were instructed to respond as quickly and accurately as possible, and completed a short practice block before the actual experiment.

Participants cared about their choices because they knew that a single randomly selected trial would be implemented for each recipient at the end of the experiment. If the participant had said yes on the selected trial, the recipient would have to eat at least three bites of the depicted food. If the participant said no, the recipient would not receive the food.

EEG data acquisition and preprocessing

EEG data were collected using a 128-channel BioSemi ActiveTwo system (Biosemi B.V., Amsterdam, Netherlands) with active electrodes with sintered Ag-AgCl tips in fitted headcaps. Evoked brain potentials were digitized continuously at 512 Hz with default low-pass at 1/5 of the sampling rate. Two additional electrodes with a 4-mm sintered Ag-AgCl pallet were placed bilaterally on the mastoids for use as references in data import. Prior to the start of data collection, electrical offsets were verified to be between –20 and 20 μV across all channels.

Data preprocessing was performed offline using the EEGLAB toolbox (Delorme and Makeig, 2004) for Matlab (Mathworks, Natick, MA). Upon import into EEGLAB, data were re-sampled to 500 Hz and re-referenced to an average reference. To address DC offsets, linear detrending was performed on the continuous data. High-pass filtering at 1 Hz and notch filtering at 60 Hz was applied to remove slow voltage drifts and electrical noise, respectively, via a two-way least-squares FIR filter. Epochs were then extracted for a 2400 ms window around the onset of the food stimulus (–200 ms pre- to 2200 ms post-stimulus onset) for initial artifact rejection.

Although participants made an equal number of decisions for themselves and the two partners, subsequent division of the data into conditions by stimulus value or stimulus attribute

219 (e.g., taste or health rating) produced unequal numbers of trials per condition due to individual
220 variations in choice. Because traditional artifact rejection methods remove whole epochs,
221 reducing the number of trials available to be averaged (Picton et al., 2000), use of these
222 techniques could lead to even greater asymmetries in the distribution of trials by condition,
223 potentially skewing the resulting average waveforms. Therefore, in lieu of traditional trial-based
224 artifact rejection, we employed independent components analysis (ICA), a method that has been
225 demonstrated to provide superior detection and removal for a variety of artefactual signals in
226 EEG (Delorme et al., 2007; Uriguen and Garcia-Zapirain, 2015) without affecting the overall
227 number of trials. Specifically, second-order blind identification (Belouchrani et al., 1997; Tang et
228 al., 2005) (SOBI) was applied to "unmix" the EEG data into a sum of temporally correlated and
229 spatially fixed components, which were then classified as task-related or artifactual based on
230 their power spectra, scalp topographies, and activity (Harris et al., 2011). Only task-related
231 components were projected back onto the scalp, allowing us to obtain artifact-corrected brain
232 signals (Jung et al., 2000) from which 1600-ms stimulus-locked epochs (–100 ms pre-, 1500 ms
233 post-stimulus onset) and 700-ms response-locked epochs (–600 pre-,100 ms post-response onset)
234 were extracted.
235
236 *EEG: Regression analysis*
237 In our first analysis, we sought to characterize the time course of value signal
238 computations, as identified by sensors and time windows in which neural activity correlated with
239 the stimulus value of the foods. For each channel, evoked data for each trial were integrated over
240 50-ms windows from 100 to 1250 ms after stimulus onset, producing a matrix of EEG responses
241 over 128 x 23 time windows in each participant. The response-locked data was likewise binned

over 30-ms windows from –600 to 90 ms before response onset, resulting in 128 x 23 sensor-time window combinations in the response-locked data. For each analysis, the EEG responses for each participant across all 128 x 23 time windows were then entered into a linear regression model as in Equation 1:

$$y_{sensor,time} = \beta_0 + \beta_1 Similar + \beta_2 Dissimilar + \beta_3 Stimulus\ Value + \beta_4 Similar * SV + \beta_5 Dissimilar * SV + \beta_6 Arousal + \beta_7 Similar * Arousal + \beta_8 Dissimilar * Arousal + \varepsilon \quad (1),$$

where $y_{sensor,\ time}$ consists of trial-by-trial data (in μV) for a particular sensor and time window, and β_0 is the average activity in the sensor. The Similar and Dissimilar covariates have a value of 1 when the decision is for the specified recipient (*Similar* or *Dissimilar*, respectively) and 0 in all other cases. The Stimulus Value covariate encodes the value of the subject's decision from 1 for Strong No to 4 for Strong Yes. The Arousal covariate, measuring the strength of preference regardless of valence (0 for Weak No or Weak Yes, 1 for Strong No or Strong Yes), was included to increase the statistical power of the linear model to identify activity associated with value (Litt et al., 2010). Finally, we computed separate covariates for the interaction of *Similar* and *Dissimilar* recipients with stimulus value and arousal, as indicated by Similar*SV, Dissimilar*SV, Similar*Arousal, and Dissimilar*Arousal. This linear regression analysis generated a set of estimated regression coefficients (i.e., beta map) for every sensor, time window, and subject. These maps were then aggregated into mixed-effect group estimates by computing one-sample t tests versus zero for each sensor and time window across all participants. The resulting *t*-statistic map allowed us to identify sensor and time window combinations in which neural activity was significantly correlated with stimulus value across participants. Results were corrected for multiple comparisons using an approximate permutation test in which the labels for all 600 trials were randomly shuffled 1000 times, and the resulting

beta maps entered into one-sample t tests from which an empirical distribution of *t* values for each sensor and time window combination was then computed.

Next, we looked at how the weighting of taste and health attributes varied by recipient. We defined an *a priori* time window of interest from 500 to 650 ms post-stimulus onset based on the time course of significant activity associated with the Stimulus Value covariate in this and previous studies (Harris et al., 2011; Harris et al., 2013; Harris and Lim, 2016). To identify sensors in this window that showed differential weighting of taste and health by recipient, we computed a regression following Equation 2:

$$y_{sensor,time} = \beta_0 + \beta_1 Health + \beta_2 Taste + \beta_3 Similar + \beta_4 Dissimilar + \beta_5 Similar * Health + \beta_6 Dissimilar * Health + \beta_7 Similar * Taste + \beta_8 Dissimilar * Taste + \beta_9 Health * Taste + \varepsilon \quad (2),$$

where the Health and Taste covariates correspond to the taste and health attribute ratings for each food item given by the individual participant, Health*Taste measures the interaction of the attribute ratings, and Similar*Health, Dissimilar*Health, Similar*Taste and Dissimilar*Taste reflect the interaction of a specific attribute with the identity of the recipient. The resulting beta maps were then compared using paired t tests of Similar*Taste – Similar*Health and Dissimilar*Taste – Dissimilar*Health to obtain sensor sets showing a significant interaction of taste and health for each recipient within the predefined time window of interest. Sensors of interest (SOI) were defined from the conjunction of sensor sets for the Similar and Dissimilar Taste – Health comparisons, and scalp topography and grand average waveforms were obtained for these SOIs.

EEG: Bayesian source reconstruction

To localize activity associated with the Stimulus Value covariate to specific brain regions, we applied distributed source reconstruction using SPM8 (Wellcome Department of Imaging Neuroscience, Institute of Neurology, London, UK). In this approach, an empirical Bayesian algorithm (Friston et al., 2008) is used to model the cortical sheet as a series of hundreds of small dipolar patches, with the constraint that a common set of underlying sources account for the evoked responses across all participants (Litvak and Friston, 2008). In contrast to traditional dipole fitting, this method does not require *a priori* assumptions about the number or spatial locations of sources. Instead, source reconstructions were first computed across the entire trial to obtain models of activity in all potential sources and time points, followed by a more specific reconstruction of the time window of interest (WOI; 500 to 650 ms post-stimulus onset) defined on the basis of previous findings and the output of our mixed-effects ERP regression analysis.

Data from all participants were entered into the same source space using a "canonical mesh" based on the SPM template head model derived from the MNI brain. Sensors were coregistered with the MRI coordinate system using a generic template of the BioSemi 128-channel layout provided with the SPM software. Sensor locations were matched to the cortical mesh via an iterative alignment algorithm, and the source space was modeled using a boundary element model.

Our analysis employed a "localization of differences" approach (Henson et al., 2007), in which we searched for a set of neural sources representing different levels of the psychological variable of Stimulus Value. Difference waveforms were computed for each sensor and participant by multiplying the average waveforms for each condition by weights used to test for a

linear (monotonically increasing) trend, and then summing across all weighted averages. To localize activity related to stimulus value computations, we used weights of (–3, –1, +1, +3) corresponding to the four levels of the Stimulus Value regressor, from Strong No to Strong Yes. To localize activity related to main effects of participant identity, contrast weights for Recipient corresponding to *Own*, *Similar*, and *Dissimilar* recipient choices were (–1, 0, 1) for the early 350 to 400 ms post-stimulus window and (-1, 1, 0) for the –300 to –180 ms pre-response window. Following reconstruction of the difference waveform for each participant, reconstructions for the WOI across participants were entered into a statistical analysis to identify statistically significant source estimates across individuals. In part due to the relatively high consistency of sensor locations across participants with the fixed cap layout used by this system, our initial analysis found large clusters of significant dipoles covering much of the brain, even at relatively rigorous family-wise-error (FWE) corrected statistical thresholds. Therefore, we chose a highly stringent threshold of $F \geq 100$ to maximize separation of source estimates into distinct clusters while retaining significant dipoles. Results were visualized in terms of maximal intensity projection, focusing on cortical generators most likely to contribute to potentials recorded at the scalp (Cohen et al., 2011).

Drift Diffusion Model Fitting: Time Varying Models

Our first modeling goal was to parameterize popular dual-process models of choice for others (i.e. anchoring and adjustment models) in a computational framework, in order to identify the most parsimonious set of parameters that accounted for patterns of choice and RT. Consistent with a growing body of work on value-based choices (Hutcherson et al., 2015; Tusche and Hutcherson, in press) we assumed that choices can be captured using a multi-attribute variant of

334 a drift diffusion model (DDM) (Smith and Ratcliff, 2004; Ratcliff and McKoon, 2008), in which
335 noisy value signals accumulate over time and a choice is made when the accumulated signal
336 crosses a pre-defined threshold for choice. In the simplest of these models, we assumed that this
337 value signal (also known as the drift rate v) at each instantaneous time point t could be described
338 as the linearly weighted sum of perceived tastiness and healthiness of the food on that trial,
339 corrupted by Gaussian noise:

340 $$v_t = \beta_{Taste} \times Taste_i + \beta_{Health} \times Health_i + \varepsilon_t \quad (3)$$

341 where β_{Taste} and β_{Health} represent the relative weights on Taste and Health, $Taste_i$ and $Health_i$
342 represent the values of Taste and Health attributes for the food shown on trial i, and ε_t is
343 distributed ~N(0, .1). We assumed that the weights on Taste and Health could vary as a function
344 of recipient (i.e., when deciding for the *Dissimilar* healthy partner, the weight on health might be
345 higher than when deciding for oneself or for a *Similar*, unrestrained partner: $\beta_{Health|Dissimilar} >$
346 $\beta_{Health|Similar}$).

347 The canonical version of the DDM assumes that β_{Taste} and β_{Health} remain constant
348 throughout the course of a single decision. However, most dual-process models assume that
349 participants make choices for similar others by anchoring first on their own preferences, and then
350 serially adjusting away from this anchor using effortful perspective taking mechanisms. This
351 suggests that β_{Taste} and β_{Health} might vary systematically over time, with early values resembling
352 weights for one's own self, and later values shifting to better reflect knowledge or assumptions
353 about one's partner. Although most descriptions of anchoring-and-adjustment models fail to
354 specify precisely the temporal dynamics of this process, we attempted to capture their basic spirit
355 using the following modifications to the standard DDM. First, we assume that the value signal at
356 instantaneous time t can be described by the following equation

$$v_t = \beta_{Taste,t} \times Taste_i + \beta_{Health,t} \times Health_i + \varepsilon_t \quad (4)$$

which is identical to Eq. 3, with the exception that β_{Taste} and β_{Health} are allowed to vary at each instantaneous time point *t.* Second, we assume that, when choosing for one's *Own Self*, β_{Taste} and β_{Health} are constant throughout the trial (i.e. $\beta_{Taste|Self,0} = \beta_{Taste|Self,\,t}$ and $\beta_{Health|Self,0} = \beta_{Health|Self,t}$). Third, we assume that when choosing for others, participants begin with their own preferences (i.e. $\beta_{Taste|Other,0} = \beta_{Taste|Self,\,0}$ and $\beta_{Health|Other,0} = \beta_{Health|Self,0}$). However, these initial weights can begin to shift after a delay *T* to a new set of weights, at a rate *r* that determines how long the shift takes once it begins. We used these two parameters to capture the common notion in dual process models that perspective-taking might take time to implement, and that it should take longer the greater the difference in value between the old and new values. Thus, the full model when choosing for one's Own Self consisted of one fixed parameter (within-trial decision noise ε, which by convention is set to .1), and 4 parameters fitted to the data: weights on health and taste ($\beta_{Taste|Self}$ and $\beta_{Health|Self}$), the choice-determining threshold ($\pm a$) and the non-decision time (*ndt*). Choices for others consisted of three fixed parameters (within-trial noise $\varepsilon = .1$, $\beta_{Taste,0} = \beta_{Taste|Self}$ and $\beta_{Health,0} = \beta_{Health|Self}$) and six fitted parameters (new weights $\beta_{Taste,\,t>T}$ and $\beta_{Health,\,t>T}$, $\pm a$, *ndt*, the transition delay *T* and the transition rate *r*).

Unfortunately, no known analytical solution to the DDM exists with time-varying drift rate parameters, rendering standard approaches to model-fitting and parameter estimation intractable. Thus, we employed a maximum-likelihood numerical simulation method similar to that employed in previous work on social decision-making (Hutcherson et al., 2015), with some important differences to speed up computation time (see Tusche & Hutcherson, in press, for details). For each participant in each condition (*Own Self, Similar*, *Dissimilar*), we began by first simulating probability distributions of choices and response times for different combinations of

parameters. We then used these probability distributions to identify the likelihood of the observed data for each parameter combination, and selected the parameter combination with the highest likelihood. Because this numerical simulation method takes a considerable amount of time that scales exponentially with the number of parameters and parameter values, we limited computational time by exploring a discrete set of values for each parameter. For the *Own Self* condition, we explored the following parameter values: threshold a = [.08, .1, .12, .14], non-decision time ndt = [.2, .3, …, .7], and $\beta_{Taste} = \beta_{Health}$= [-.02, -.01, -.005, 0, .005, .01, .02, ….14]. Parameter values for the Similar and Dissimilar partner conditions were identical except that the fitted values of β_{Taste} and β_{Health} represented the post-adjustment weights on Taste and Health after shifting away from the egocentric Self weights (estimated from the Self condition), and we included two additional time parameters to describe this shift: a delay parameter T = [0, .1, …, .5] sec, and a rate parameter r = [1.2, 2.4, 4.8, 9.6, 1000] describing how quickly old values shifted to new values following the delay. For example, a rate r = 1.2 suggests that it takes 1 second to shift 1.2 value units, or, equivalently, 250ms to shift .4 units. A rate r = 1000 indicates an instantaneous shift.

Using these values, we performed model fitting and model selection in the following manner. We first estimated the best-fitting parameter values for each participant's choices in the *Similar* and *Dissimilar* partner conditions separately, estimating the full model with six free parameters. We then estimated a reduced, four-parameter model with only base parameters allowed to vary, T fixed at 0 (i.e. no early egocentric bias) and r fixed at 1000 (no gradual shift). Then, for each subject, we calculated the Bayesian Information Criterion (BIC) for each model based on the estimated likelihood of the data using the best-fitting parameter values. The winning model was determined based on which model had the lowest BIC value for the largest

number of subjects, as well as the lowest BIC value when summing over all subjects. As we describe in greater detail in the results section below, this procedure identified the four-parameter model as the most parsimonious model to account for the data.

Drift Diffusion Model Fitting: Constant Value Models

Because the analyses described above found no evidence for a time-varying adjustment process, all subsequent DDM estimation used canonical versions of the DDM, and was performed using a recently developed software package freely available in Python (Wiecki et al., 2013). Models were estimated using a Bayesian hierarchical framework, with Markov chain Monte Carlo (MCMC) sampling methods employed to estimate a joint posterior distribution of the model parameters. Hierarchical Bayesian estimation allows individual participant estimates to be constrained by a group distribution, but also to vary to the extent that their data demonstrate separation from the data of others. Estimation used non-informative priors: all priors were uniform distributions over large intervals of possible parameter values.

Several different DDM specifications were fit to the data. All of the DDM specifications assume the drift rate is a linear sum of weighted Taste and Health ratings, where the weights are allowed to vary by condition (*Own*, *Similar*, *Dissimilar*):

$$v = \beta_{1Own} I(Own) Taste + \beta_{2Own} I(Own) Health + \beta_{1Similar} I(Similar) Taste + \beta_{2Similar} I(Similar) Health + \beta_{1Dissimilar} I(Dissimilar) Taste + \beta_{2Dissimilar} I(Dissimilar) Health \text{ , (5)}$$

where I(Recipient) is an indicator function for each of the three conditions. The first model (M1) only allowed drift rate, as specified in Equation 3, to vary by task condition. All other parameters (*ndt*,*a*,*z*) were allowed to vary by subject, but did not vary within subject. The second model

(M2) included drift rate as in M1, but also allowed the barrier parameter to vary with task condition, according to

$$a = \beta_0 + \beta_1 I(Similar) + \beta_2 I(Dissimilar). \quad (6)$$

This model allowed for the possibility that, in addition to weighting attributes differently by recipient, individuals may also employ different thresholds depending upon the recipient. A third model (M3) considered the same drift rate as in M1, but also allowed the starting point, or bias, parameter *z* to vary with task condition, similar to Equation 4. This model did not allow barrier to vary with task condition. A fourth model (M4) allowed drift rate, barrier, and starting point to vary within participants. In all DDM specifications, the non-decision time parameter *ndt* was modeled to vary across participants, but not within participants.

We used two methods to compare fits of the various DDM specifications. First, we used the Deviance Information Criterion (DIC), a flexible measure for goodness-of-fit in hierarchical Bayesian models (Spiegelhalter et al., 2002). The DIC combines a measure of deviance (i.e., lack of fit) with a penalty for model complexity. A lower DIC represents a better model fit, and differences in DIC greater than 10 are typically thought to reflect significant differences (Spiegelhalter et al., 2002). Second, we compared observed data to data generated using random samples from the sampled posteriors (Wiecki et al., 2013). For each of the four models, 100 samples for each experimental subject were created. The squared error between each simulation and observed data was computed for both choices and RT, with the mean squared error (MSE) computed across the 100 runs. These statistics are reported for each model in Table 1.

Model convergence was assessed using the Gelman-Rubin (G-R) $\hat{R}$ statistic (Gelman and Rubin, 1992). The $\hat{R}$ statistic compares within-chain and between-chain variance of different

runs of the same model. Perfect convergence would be demonstrated with an $\hat{R}$ equal to 1. The $\hat{R}$ statistic was computed for all of the model parameters based on five runs of the model.

Another advantage of Bayesian estimation is that it is straightforward to compare differences in parameter estimates. Significance inference is possible using the posterior distributions generated from sampling. To compare coefficients to the null hypothesis ($\beta = 0$) the percentage of the N=10000 samples greater than zero can be assessed. Similarly, to determine whether or not a regression coefficient is greater than another, the percentage of the difference between the N=10000 samples that is greater than zero can computed.

Results

In this experiment, we investigated the neural and computational bases of decisions for self and others by measuring behavioral and ERP responses as participants with unrestricted diets made food choices for themselves and two partners: a similar partner with unrestricted preferences, and a dissimilar self-identified healthy eater (*Own* self, *Similar* other, and *Dissimilar* other conditions, Figure 1). First, participants rated 250 different appetitive snack foods on their perceived tastiness and healthiness. Second, for a subset of 200 foods selected to vary in taste and health, they were asked to decide whether they would select the pictured food for consumption after the experiment, making these choices once for each of the three recipients. To ensure that choices were incentive compatible, at the end of the study, one random trial was selected for each recipient and the participant's choice on these trials was realized.

To characterize the neural and behavioral correlates of this social decision scenario, we performed a series of analyses as detailed in the following sections. First, we analyzed the behavioral choice and RT data to verify that participants were taking recipients' preferences into

consideration when making their decisions, and to replicate patterns previously associated with egocentric correction mechanisms. Next, we examined the stimulus-locked ERP data to find neural signals associated with stimulus value computations, further assessing how taste and health attributes were incorporated for each recipient during value integration. To determine how neural activity differed as a function of recipient, we compared ERP responses in each condition, time-locked to either the stimulus or the keypress response.

Although these analyses gave us a set of ERP components that correlated with different aspects of the decision process, they were blind to the specific cognitive operations indexed by these neural markers. Thus, to shed further light on the nature of these signals, we developed a set of novel multi-attribute computational models of choices for self and others based on extensions of the drift diffusion model (Ratcliff et al., 2016) and applied it to our event-related data. The primary assumption of these models is that weights on attributes like taste and health shape the evidence accumulated in favor of accept or reject responses. These weights can vary, not only as a function of choice recipient, but also as a function of time (i.e., biased toward automatic, egocentric defaults early on and then shifting over time with the application of controlled perspective taking). To test this latter assumption, we first implemented computational models in which the construction of value was allowed to vary systematically over time within a decision, and used formal model comparison and selection procedures to test whether and when this shift might occur. Second, having identified the simplest behavioral computational model to account for patterns of choice and RT, we then attempted to link trial-by-trial fluctuations in neural response to trial-by-trial variation in specific cognitive parameters such as the rate of evidence accumulation and threshold for response. Finally, applying our neurocomputational model to the behavioral data, we ran a series of simulation exercises demonstrating that

distributions of choice and RT which appear consistent with default egocentric biases and slow effortful correction models of decision making can in some cases be explained without a correction mechanism, and assuming only relatively egocentric attribute weighting and value integration.

Behavior: Observed choice and RT

To verify that participants made inferences consistent with their partner's preferences, we first examined whether recipient identity influenced the likelihood of making a healthy choice (i.e., accepting/rejecting items rated high/low on health, Figure 2A). As expected, participants made healthier choices when choosing for the *Dissimilar* "healthy eater" compared to choosing either for *Own* self (paired-t_{37} = 9.19, $P = 5\text{x}10^{-9}$) or the *Similar* other (paired-t_{37} = 10.49, $P = 1\text{x}10^{-12}$). Participants made marginally *fewer* healthy choices for the *Similar* other (paired-t_{37} = 1.87, P = .069).

We also asked how often participants made the same choice for themselves and their partner, one way of testing for egocentric responses. Participants made the same accept or reject choice for the *Similar* other as for themselves on 72±11% of trials, but chose the same significantly less often (60±17% of the time) when choosing for the *Dissimilar* other (paired-t_{37} = 3.69, P = .0007). These results suggested that participants tend to choose similarly for both recipients, with a more pronounced bias for the *Similar* other.

Next, we examined RTs for evidence that decisions for others might require additional computational resources. We analyzed behavior in two ways: average RT across all choices, and RT as a function of choice similarity between self and other. In line with the idea that choosing for others is more computationally costly, we observed significant differences in mean RTs

517 depending on the recipient's similarity (Figure 2B). Participants were fastest when choosing for
518 themselves (mean = 1.11 s, SD = 0.18) and slowest when choosing for the similar other (paired-
519 $t_{37} = 7.59$, $P = 5x10^{-9}$), with choices for the dissimilar partner lying in between and significantly
520 different from the other two conditions (both paired-$t_{37} > 2.17$, both $P < .036$).

521 A critical finding from previous research is that individuals take longer to choose for
522 similar others when making choices that differ from their own preferences, but that this effect is
523 reduced when choosing for dissimilar others (Epley et al., 2004; Tamir and Mitchell, 2013). As
524 seen in Figure 2C-E, we replicated this pattern, observing longer RTs when choices diverge from
525 *Own* preferences, for both *Similar* (different choice: mean = 1.37 s, SD = 0.25; same choice:
526 mean = 1.22 s, SD = 0.28; paired-$t_{37} = 7.90$, $P = 2x10^{-9}$) and *Dissimilar* (different choice: mean
527 = 1.23 s, SD = 0.26; same choice: mean = 1.14 s, SD = 0.23; paired-$t_{37} = 3.35$, $P = .002$)
528 conditions. This effect was marginally more pronounced in choices for the *Similar* partner
529 compared to the Dissimilar partner (paired-$t_{37} = 1.75$, $P = .089$), in keeping with prior work
530 (Tamir and Mitchell, 2013).

531 Intriguingly, however, we also found a slowing effect when making choices for one's self
532 that diverged from the choices made for partners (*Own* vs. *Similar*: mean $RT_{Different}$ = 1.22±0.20
533 s, mean RT_{Same} = 1.09±0.17 s, paired-$t_{37} = 6.27$, $P = 2x10^{-5}$; *Own* vs. *Dissimilar*: mean $RT_{Different}$
534 = 1.23±0.26 s, mean RT_{Same} = 1.14±0.23 s, paired-$t_{37} = 3.35$, $P = .002$). This analysis has not
535 been reported previously, to our knowledge, and raises important questions about the most
536 parsimonious explanation of RT differences for divergent choices, as we discuss in greater detail
537 with respect to our computational simulation results below.

538

539 *ERP: stimulus value integration*

540 Given that participants adjusted their choices to reflect the recipient's preferences, a
541 further question is when and how relevant value signals emerge in the brain. Although fMRI
542 studies have identified overlapping regions of VMPFC representing value for both oneself and
543 others (Nicolle et al., 2012; Janowski et al., 2013), some dual-process models suggest that these
544 signals should take longer to construct for others. Therefore, the high temporal resolution of ERP
545 is of crucial importance in determining the time course of stimulus value integration when
546 choosing for oneself versus others. We began by identifying neural correlates of stimulus value
547 computation, which previous neurophysiological studies of choice for oneself have identified
548 from approximately 500 to 650 ms after stimulus onset, localized to regions including the
549 VMPFC (Harris et al., 2011; Harris et al., 2013; Harris and Lim, 2016).

550 We applied a linear regression analysis to the ERP data in order to identify neural activity
551 correlated with the decision made in each trial (1 = Strong No to 4 = Strong Yes) across
552 participants. As shown in Figure 3A, ERP data was binned over 50-ms windows from 100 ms to
553 1200 ms after stimulus onset, for all 128 sensors grouped by scalp location. Data were
554 permutation-corrected to account for multiple statistical comparisons. This analysis revealed
555 significant main effects of stimulus value, regardless of recipient, at two major time windows
556 leading up to the time of choice. Consistent with previous studies, the earliest major cluster of
557 value-related activity occurred from approximately 500 to 650 ms after stimulus onset (Figure
558 3A, green box), with additional activity in roughly the same set of sensors re-emerging from 700
559 to 850 ms post-stimulus onset (Figure 3A, blue box). Distributed source reconstruction of scalp
560 topography for these two time windows localized the stimulus value signal to regions including
561 VMPFC, with a particularly pronounced localization to VMPFC in the 500-650 ms time window
562 (Figure 3B, circled). Although the coarse spatial resolution of ERP precludes detailed

563 specification of sources, the sources found here closely resemble those from previous fMRI
564 studies (Figure 3B, top inset), as well as prior ERP localizations (Figure 3B, bottom inset) within
565 the same latency range (Harris et al., 2013; Harris and Lim, 2016).

566 Given the overlapping sensor distributions and source localizations for the earlier and
567 later time periods, what differentiates neural value integration during these two windows? To
568 address this question, we examined stimulus value computations as a function of recipient
569 identity using the conjunction of significant sensors 500-650 ms and 700-850 ms after stimulus
570 onset (Figure 3C). Grand average waveforms from central sensors (Figure 3C, left) revealed a
571 clear linear ordering from Strong No to Strong Yes for all recipients between 500 and 650 ms
572 post-stimulus (Figure 3C, shaded green region). In contrast, activity in the later 700-850 ms
573 window demonstrated a strong "self-relevance" effect (Grueschow et al., 2015): the strongest
574 Stimulus Value responses were observed for one's *Own* self, perhaps reflecting sustained
575 attention to one's own choices, with diminished responses for *Similar* and *Dissimilar* partners
576 (Figure 3C, shaded blue region). In line with these observations, covariates representing the
577 interaction of stimulus value by recipient, computed separately for each partner, showed no
578 significant effects from 500 to 650 ms post-stimulus, but significant negative interactions in the
579 later time range. Visualizing these effects at the scalp (Figure 3D), we found that, relative to the
580 main effect of stimulus value (Figure 3D, top), interactions of recipient and stimulus value were
581 significantly negative for both *Similar* (Figure 3D, middle) and *Dissimilar* (Figure 3D, bottom)
582 recipients in the later time window. Thus, we did not find stronger delayed value representations
583 during decisions for others, as would be expected if participants required additional time to
584 construct others' preferences. Instead, later value responses more likely reflect sustained
585 attention and/or arousal to choices with a direct impact on one's own outcomes.

586

587 *ERP: attribute weighting by recipient*

588 In line with the hypothesized role of VMPFC in context-dependent value integration
589 (Hare et al., 2009), ERP value signals from roughly 500 to 650 ms post-stimulus have previously
590 been shown to reflect increased weighting of health attributes when participants are incentivized
591 to exercise dietary self-control (Harris et al., 2013). Thus, we predicted that neural activity in this
592 time window would show differential weighting on taste and health depending on the recipient of
593 the choice. To test this, we computed a second regression identifying sensors in which neural
594 activity significantly correlated with the interactions of *Similar* and *Dissimilar* recipient by Taste
595 and *Similar* and *Dissimilar* recipient by Health. The resulting beta maps were then compared
596 using paired t-tests to find sensors where the relative weighting of taste (Figure 4A, left) and
597 health (Figure 4A, middle) varied by recipient from 500 to 650 ms after stimulus onset.
598 Difference plots of scalp topography in this time window identified a set of central sensors
599 (Figure 4A, right) for the interaction of taste and health in both *Similar* and *Dissimilar*,
600 overlapping those associated with stimulus value in our initial analysis. Sensors of interest
601 (SOIs) were formally defined via the conjunction of sensors associated with significant
602 weighting on Taste – Health in both *Similar* and *Dissimilar* recipient conditions. As expected,
603 grand average waveforms for these SOIs demonstrated the clearest parametric effect of taste
604 when deciding for one's *Own* self versus the two partners (Figure 4B, left). In contrast, the linear
605 ordering of health showed the greatest effect for the *Dissimilar* healthy eater and negligible
606 distinction by health for one's *Own* self (Figure 4B, right). Confirming these effects, calculations
607 of the linear contrast of the ERP response to taste (Figure 4C) and health (Figure 4D) clearly
608 showed greatest weighting of taste in decisions for one's *Own* self and greatest weighting of

health for the *Dissimilar* other. A repeated-measures ANOVA on the computed linear contrast weights with Attribute (Taste/Health) and Recipient (Own/Similar/Dissimilar) as covariates likewise found a significant main effect of Attribute ($F(1,35) = 10.1$, $p = 0.003$) and a significant interaction of Attribute x Recipient ($F(2,70) = 5.05$, $p = 0.009$), with the latter reflecting a significant linear contrast ($F(1,35) = 8.39$, $p = 0.006$). These results support the idea that value integration from approximately 500 to 650 ms post-stimulus reflects differential attribute weighting for oneself and others.

ERP: neural signals related to recipient identity

The findings described above bolster the idea that decisions for others recruit similar value computation mechanisms as decisions for oneself, on the same time scale, regardless of how dissimilar the recipient's preferences may be. However, these results raise an additional question: how and when does the brain modify value computations to distinguish the intended recipient of the choice? To address this issue, we next looked for neural activity that differentiated recipient identity, using ERP data time-locked to both stimulus and response.

Some versions of a dual-process account suggest that inhibition of egocentric biases should emerge relatively late in the process and, because similar individuals more strongly activate egocentric biases that need correcting, such inhibition should be more pronounced for the *Similar* other (Tamir and Mitchell, 2013). In contrast, other research suggests attention and perspective taking mechanisms should be most pronounced for the *Dissimilar* other, whose preferences differ most markedly from one's *Own* self (Silani et al., 2013). Given that we found a similar time course of value integration by recipient, we hypothesized that this perspective-taking and adjustment process might actually occur *early,* prior to or during the window of

632 stimulus value computation (i.e., prior to 500 to 650 ms post-stimulus). Previous neuroimaging
633 research has suggested that regions associated with social cognition, such as TPJ and superior
634 temporal sulcus (STS), play a key role in directing value integration in VMPFC during social
635 decisions (Hare et al., 2010; Hutcherson et al., 2015; Strombach et al., 2015). Therefore, we
636 further predicted that any differences would localize to regions including TPJ.

637 To test these predictions, we computed a linear regression with separate dummy-coded
638 indicator variables for *Similar* and *Dissimilar* recipient; the results of this analysis from 100 to
639 600 ms after stimulus onset, our *a priori* time window of recipient computation, are shown in
640 Figure 5A. Although the covariate for *Similar* recipient (Figure 5A, left) was largely non-
641 significant during this time window, we found significant ERP activity for the *Dissimilar*
642 recipient from approximately 350 to 400 ms post-stimulus onset (Figure 5A, right). Average
643 waveforms for these sensors and time window (Figure 5B) revealed a positive response for the
644 *Dissimilar* condition relative to one's *Own* self, localized to sources including posterior superior
645 temporal sulcus (STS) and TPJ (Figure 5B, right). Consistent with previous studies (Saxe, 2006;
646 Andrews-Hanna et al., 2010; Hare et al., 2010; Hutcherson et al., 2015), these results suggest a
647 mechanism by which brain networks involved in mentalizing about others may communicate
648 with valuation regions in order to adjust attribute weights during value integration.

649 Although pre-value signals differentiated the *Dissimilar* other from both *Own* self and
650 *Similar* other trials, we also sought to test predictions of several dual-process models that there
651 may also be a late adjustment process, unique to choices for *Similar* others, that delays choices
652 and corrects egocentric values to account for differing preferences. Although we did not find
653 evidence for late value integration signals when deciding for *Similar* others (see "Stimulus value
654 integration" results above), we nevertheless asked whether there was a main effect of recipient

identity in late-emerging response-locked ERP signals, as might be predicted by some dual-process models. Intriguingly, a linear regression on ERP data time-locked to the keypress response revealed a significant main effect of *Similar* recipient from approximately –300 ms to –180 ms pre-response (Figure 5C), reflecting a more positive deflection for *Similar* relative to *Own* and *Dissimilar* (Figure 5D). To shed light on the nature of this process, we performed source localization from –300 to –180 ms pre-response. In this time window, the main effect of *Similar* recipient was predominantly localized to the intraparietal sulcus (IPS), close to an area previously identified as being more activated when choosing for others (Janowski et al., 2013). In contrast, significant main effects of *Dissimilar* recipient in this time window were largely confined to the period immediately prior to response (–120 to 0 ms pre-response), and thus are more likely to reflect the initiation of movement potentials associated with the motor response.

Computational Modeling

As described above, our analysis of the time course of value integration suggests that a *single* valuation mechanism, localized to the VMPFC, computes stimulus values using weighted attribute integration for both self and others, with similar temporal dynamics. Yet the presence of both early- and late-emerging components in TPJ and IPS that were specific to choosing for others is fully consistent with dual-process models of choice in which perspective-taking mechanisms alter value computations to reduce egocentric biases. This raises an important question: what is the most parsimonious computational framework to account for both the behavioral and neural data?

To address this issue, we used the power of formal model comparison and selection procedures to identify the most parsimonious computational model of decision making for oneself versus others, and then explored how changes in parameter values across choices for self and others shed light on neural and behavioral responses. We began by specifying a multi-attribute variant of the DDM that allowed us to capture basic assumptions of dual-process accounts, which suggest that the construction of value should vary in systematic ways over the course of a decision. More specifically, we assumed that weights on taste and health attributes influence the overall drift rate (v), and that these weights should be egocentrically biased early on during a decision but shift gradually after a delay to a new set of weights that reflect a participant's assumptions about the preferences of their partner after deliberation. We compared this model to a nested model in which, when choosing for others, participants simply begin at the outset with a set of weights that reflect their assumptions about the other person's preferences, with no delay or gradual adjustment process (see Methods for details). Remarkably, for the *Similar* condition, the nested model with no time-varying parameters had a lower BIC value combining over all subjects (1.2159×10^5) compared to the time-varying model (1.2189×10^5), as well as a lower BIC value for 36 out of 38 individual subjects. Conclusions were largely similar using the more liberal Akaike Information Criterion (AIC) instead of BIC. We arrived at identical conclusions when examining choices for the *Dissimilar* other (total BIC of the simple model = 1.1487×10^5, total BIC of the time-varying model = 1.1518×10^5).

Having shown that a simple DDM provided a more parsimonious fit to the data, we then sought to determine how the values of different model parameters might change as a function of choices for *Own Self, Similar,* and *Dissimilar* others. Specifically, we implemented a multi-attribute version of the DDM with five parameters: weights on the taste and health attribute in

the drift rate (v), threshold for choice (a), starting point bias (z), and non-decision time. We fit four different versions of the DDM to the data, in which drift rate, threshold, and starting point bias were allowed to vary depending on the choice recipient (Table 1). The best-fitting model, as assessed by both lower DIC values and lower MSE (M2; Table 1) suggested that, as expected, weights on health and taste varied significantly by recipient. On average, participants weighted both the health and taste attributes more similarly to themselves for the Similar individual than for the Dissimilar individual (Table 2). However, in all cases there were significant pairwise differences between attribute weights for different recipients. Taste ratings were weighted highest for *Own* self, somewhat less for the *Similar* other, and not at all for the *Dissimilar* other (all comparisons: 100% of the difference in posteriors > 0, i.e., all P-values = .000). Health ratings were weighted highest for *Dissimilar*, significantly less for the *Similar* other, and least for *Own* self (all comparisons significantly different, all P = .000).

Although weights on taste and health attributes differed significantly on average during choices for both *Similar* and *Dissimilar* others compared to *Own* self, most models of choice assume that participants also show egocentric biases, using their own preferences when making choices for others (e.g., Devaine and Daunizeau, 2017; Tarantola et al., 2017). To test this possibility, we theorized that if people do use their own preferences to some degree when choosing for others, then individual differences in the weights estimated for Taste and Health attributes in *Own* choices should predict the weights estimated for these attributes when choosing for others, particularly when those preferences are relevant to the choice at hand. This prediction was robustly confirmed. Individual weights on taste for one's *Own* self correlated strongly with weights on taste for the *Similar* other (r_{36} = .58, P = .0002) but not for the *Dissimilar* other (r_{36} = .07, P = .66). Individual weights on health for one's *Own* self correlated with weights for both

723 the *Similar* other (r_{36} = .57, P = .0002) and *Dissimilar* other (r_{36} = .48, P = .003). Thus, our best-
724 fitting model strongly supports the existence of an egocentric bias when making choices for
725 others.

726 Intriguingly, the best-fitting model also suggested significant variation in the threshold
727 parameter a as a function of choice recipient. Participants adopted greater caution when choosing
728 for others compared to themselves, with the highest threshold associated with choosing in the
729 *Similar* other condition. We speculate that these thresholds are adjusted to accommodate greater
730 uncertainty about the appropriate choice, and that this uncertainty may have been highest for the
731 *Similar* other, a point we return to in the Discussion. In contrast to attribute weights and
732 threshold, starting point (i.e. response bias) did not significantly differ from an unbiased value of
733 0.5 (11.9% of posterior > 0.50, i.e., P = .119) and was similar for all recipients.

734 To confirm the ability of the DDM to successfully capture both observed choice and RT
735 data, posterior predictive simulations (Wiecki et al., 2013) were generated using 100 randomly
736 selected samples from the posterior, effectively generating 100 synthetic datasets. Posterior
737 predictive checks using this simulated data confirmed the ability of the model to recreate
738 acceptance rates and RTs at both the group and individual level. Pearson correlations between
739 the true data and synthetic data for participant-level average data were for high for both
740 acceptance rates (*Own*: 0.863, *Similar*: 0.750, *Dissimilar*: 0.755) and RT (*Own*: 0.934, *Similar*:
741 0.921, *Dissimilar*: 0.942). Importantly, convergence statistics suggested stable parameter
742 estimates across all parameters in the hierarchical model (Table 2).

743

744

745

Combined ERP-model results

We next sought to validate our model not only through behavior, but by linking specific ERP components to specific model parameters. We predicted that if value signals in the VMPFC measured on-line during decision making between 500-650ms represent the most proximal input into the evidence accumulation process, fluctuations in this signal should be directly related to variation in the model-estimated influence of taste and health on the drift rate, *even after accounting for behavioral ratings* collected after the fact. To test this prediction, we entered trial-by-trial stimulus-locked ERP data from our SOIs and 500-650 ms time window of interest (Figure 6A) into the M2 specification for the DDM, interacted with both Health and Taste ratings. Note that stimulus-locked signals in the VMPFC were identified based on their association with health and taste ratings collected independently of the choice, and are here assumed to be an *input* into the accumulation process, and not an output of it.

As predicted, during choices for both *Own* self and *Similar* other, the amplitude of the ERP value response predicted a significantly higher influence of Taste on the drift rate when choosing for *Own* self and *Similar* other (Figure 6B, 100% of the posteriors for the interaction > 0, i.e., $P = .000$), but not when choosing for the *Dissimilar* other ($P = .380$). *Own* and *Similar* Taste*ERP effects were not significantly different from each other (*Own* > *Similar*, P=.118), but were both significantly greater than *Dissimilar* ($P = .000$). By contrast, the amplitude of the ERP response significantly enhanced the influence of the Health attribute when choosing for the *Dissimilar* other ($P = .000$), and this effect was significantly greater than for *Own* (P=.001) or *Similar* ($P = .000$) choices (Figure 6C). These results strongly support the idea that VMPFC value signals from 500-650ms contribute to choice by influencing the accumulation of attribute evidence toward a choice.

769 If attribute representations in the VMPFC contribute to evidence accumulation, shifting
770 to represent preferences of the choice recipient, what drives changes in those attribute
771 representations, particularly during choices for the *Dissimilar* other? Based on previous research
772 implicating TPJ and STS in directing VMPFC value integration during social decision (e.g., Hare
773 et al., 2010), we speculated that the ERP response for *Dissimilar* choices from 350-450 ms post-
774 stimulus may play a role in perspective taking and attribute weighting. If so, the strength of this
775 response across individuals should predict individual differences in alteration of the weights on
776 taste and/or health. To test this hypothesis, we computed the mean differences in the amplitude
777 of this response for *Dissimilar – Own* and *Similar – Own*, and correlated this difference with
778 differences in taste and health weights for the same contrast. Consistent with the idea that this
779 response may serve to inhibit the use of egocentric preferences, larger ERP amplitude from 350-
780 400 ms across participants significantly predicted reduced weighting on taste for the *Dissimilar*
781 recipient (Spearman's rho = -.41, P = .01). No other correlations were significant, suggesting a
782 specific role for this signal in reducing egocentric use of taste preferences.

783 We next sought to use our computational model to understand the nature of the response-
784 locked signals localized to the IPS, which showed the largest difference in signal for *Similar*
785 others (Figure 6D). Notably, applying our computational model to the behavioral data suggested
786 that, rather than resulting from serial correction mechanisms, longer RTs on average when
787 choosing for others could result in part from the adoption of different response thresholds
788 relative to the self, particularly in the case of the *Similar* other (Figure 6E). If so, we would
789 predict that response-locked ERPs localized to the IPS may contribute to adjusting the *response*
790 *threshold,* rather than correcting egocentric value signals.

791 Therefore, we directly tested whether this neural response-locked component influenced
792 the threshold parameter by entering the trial-by-trial ERP data from the response-locked
793 posterior SOIs and –300 to –180 ms time window of interest into the M2 specification for the
794 DDM, interacted with the response threshold. Results confirmed a significant relationship
795 between neural response in the IPS and the height of the response threshold (Figure 6F).
796 Moreover, adding this regressor improved model fit (DIC = 41421.1, compared to DIC= 41625.6
797 for an equivalent to M2 with the same set of trials used in the response-locked ERP version of
798 M2). Importantly, the estimate of the ERP regressor was strongly positive (P = .000), with no
799 significant interaction as a function of recipient. Although the polarity of the observed ERP
800 signal depends on a variety of factors including reference electrode, sensor location, and cortical
801 anatomy, the positive influence of this ERP component on the barrier coefficient is in line with
802 the more positive amplitude observed in the response-locked data when choosing for the *Similar*
803 other compared to the other two conditions.
804
805 *Simulation exercise: RTs for same and different choices*
806 Above, we demonstrate that the best-fitting parameters of a simple weighted-integration,
807 constant-value DDM can account for overall choice and RT patterns, and can be linked to
808 specific ERP components. Notably, this model supports the idea of egocentric biases, but does
809 *not* include a late-acting mechanism for adjusting preferences when choice for self and similar or
810 dissimilar others diverge. This contrasts with dual-process models such as anchoring-and-
811 adjustment, which are primarily supported by behavioral and RT data. We thus asked whether
812 our model could generate the RT patterns typically associated with an anchoring-and-adjustment
813 mechanism: namely, longer RTs when choices for Similar others diverge from choices for

814 oneself. To do this, we generated 160,000 simulated food choices for each recipient (*Own*,
815 *Similar*, *Dissimilar*) based on the 16 possible combinations of health and taste ratings. Then, for
816 each pairing of recipients (i.e., *Own* vs. *Similar*, *Own* vs. *Dissimilar*, *Similar* vs. *Dissimilar*), we
817 determined how often foods with each combination of taste and health rating led to similar or
818 different simulated choices (Figure 7), as well associated RTs. All statistical comparisons of the
819 simulated RTs were performed using Bayesian analysis incorporating MCMC estimation to
820 generate distributions of likely means and standard deviations (Kruschke, 2013). A *P*-value of
821 zero thus represents completely non-overlapping simulated distributions.

822 As expected, model simulations with the fitted parameters suggested that choices for
823 *Own* self and *Similar* other agree more frequently (68% of simulated choices) than for *Dissimilar*
824 other (52% agreement). More importantly, the simulated data also clearly replicate the RT
825 patterns observed both in previous work and in the present study (Figure 7A, top). When
826 comparing decisions for the *Similar* recipient to one's *Own* choices, RTs were considerably
827 faster for same versus different choices ($P = .000$). When comparing decision for *Dissimilar*
828 other to one's *Own* choices, RTs were also on average faster for same versus different choices,
829 although the differences were notably smaller ($P = .073$). Finally, when comparing choices for
830 one's *Own* self to decisions for others, we replicated the novel observation that decisions for the
831 self that result in the same response as that made for similar others *also* tend to be made faster
832 than choices for the self that differ (P = .000).

833 To provide additional insight into *when* choices converge or diverge, and why these are
834 consistently associated with different RTs, we compared the projected value of a food for two
835 given recipients to the likelihood that the model simulations make different choices about that
836 food (Figure 7B). We divided foods by the sixteen possible combinations of health and taste

837 ratings (e.g., health = 3 and taste = 2). Using health and taste weights derived from model M2,
838 we mapped the projected value of the food versus the percentage of different choices. As
839 expected, this analysis shows that the values of different foods fall closer to the diagonal when
840 comparing choices for one's *Own* self to a *Similar* other, suggesting that these values are more
841 tightly related (Figure 7B, left). In this case, choices diverge more frequently for options with
842 intermediate overall values (i.e., ratings of Weak No or Weak Yes on both taste and health
843 attributes vs. Strong No or Strong Yes), largely due to noisier choices in the face of indifference.
844 In contrast, when comparing choices made for *Own* self and a *Dissimilar* other (Figure 7B,
845 middle), the values of the food are less correlated, and a greater percentage of divergent choices
846 are observed at the extremes (e.g., very unhealthy but very tasty, or vice versa), due to the
847 differences in attribute weights. Divergent choices in this case are also less likely to be errors.
848 Next we examined the extent to which observed patterns of choice divergence correspond
849 to our model predictions (Figure 7C). We first used multiple regression to estimate the
850 coefficients on health and taste for choices made in the *Own*, *Similar*, and *Dissimilar* conditions,
851 separately for each subject. From these coefficients, we estimated the overall decision value for
852 each subject of each food in each condition. Then, for each of the 16 combinations of health and
853 taste ratings, we calculated the average decision value across all subjects for that combination,
854 separately for each condition. Finally, we also calculated the percentage of the time that choices
855 diverged for two recipients, separately for each of the 16 combinations. As can be seen from
856 Figure 7C, the data hew closely to the simulated predictions. Specifically, there is a strong
857 correlation between the value for one's *Own* self and the value for *Similar* other, and the largest
858 difference between choices for *Own* and *Similar* occur for values close to 0 (Figure 7C, left). In
859 contrast, when comparing values and choices for one's *Own* self and the *Dissimilar* other, the

most divergent choices occur at the extremes of conflict between health and taste (Figure 7C, middle). Comparison of choices for *Similar* and *Dissimilar* lie in between (Figure 7C, right).

Thus, our model explains the longer RTs we observed when making different choices for similar others, compared to dissimilar others. Put simply, in this paradigm people choose differently for similar others in the same cases where they would be less certain what to choose for *themselves.* Our simulations suggest that the extra deliberation time and divergent choice in these trials emerges organically from increased uncertainty within a single decision process, despite giving the appearance of resulting from a serial, slow-to-activate corrective process.

Discussion

To what extent do decisions for oneself and others rely on shared neurocomputational mechanisms versus recruiting additional slow or deliberative mechanisms (Epley et al., 2004; Tamir and Mitchell, 2013)? Do increases in response time for others reflect effortful correction or uncertainty within a process of stochastic evidence accumulation? Here we exploited the high temporal precision of ERP and the power of computational model fitting (Ruff and Fehr, 2014; Crockett, 2016) to generate novel insights into these important questions.

Consistent with previous work (Nicolle et al., 2012; Janowski et al., 2013), our results strongly support the existence of a shared value integration process for self and others, and further suggest that this process follows similar temporal dynamics. Neural value signals for other recipients emerged within the same temporal window as those for oneself, approximately 500-650 ms after stimulus onset and localized to regions including VMPFC. Importantly, however, these value signals represented taste and health attributes differently depending on the decision context, in line with previous data on dietary self-control (Harris et al., 2013).

883 Moreover, we demonstrated a link between trial-level fluctuations in the ERP value signal and
884 trial-by-trial differences in the process of evidence accumulation associated with each recipient.
885 Whereas VMPFC signals promoted taste considerations when deciding for oneself or the similar
886 other, these same signals promoted health attributes when deciding for the dissimilar, healthy
887 eater. Notably, these signals emerged in the stimulus-locked data more than 400 ms prior to the
888 average response time, suggesting that they represent an input into brain systems associated with
889 choice selection (Hare et al., 2011) rather than directly implementing accumulation-to-bound and
890 choice at the motor level. However, in light of previous work linking VMPFC response to choice
891 selection processes (Hunt et al., 2012; Strait et al., 2014), as well as other data demonstrating
892 rapid interactions between VMPFC and sensorimotor systems (Harris and Lim, 2016), further
893 research will be necessary to fully disentangle the relationship between ERP value signals and
894 evidence accumulation.

895 This shared VMPFC mechanism might also explain, in part, the robust and consistent
896 evidence for egocentric biases when choosing for others (Ross et al., 1977; Devaine and
897 Daunizeau, 2017; Tarantola et al., 2017). In our study, we found some evidence that people use
898 their own preferences to guide choices for others, particularly when those preferences may be
899 relevant. One's own weights on *both* taste and health predicted weights used when choosing for a
900 similar other, whereas when choosing for a dissimilar, healthy eater, only one's own health
901 preferences predicted choice. Thus, we find not only that people use their own preferences, but
902 also that they do so selectively based on inferences about the intended recipient.

903 Our results also support the use of additional perspective-taking mechanisms, particularly
904 when deciding for people with different preferences from one's own. We observed an ERP
905 component specific to choosing for the *Dissimilar* recipient from 350 to 400 ms after stimulus

onset, just before the time window associated with stimulus valuation. This signal was localized to posterior temporal areas near the temporoparietal junction (TPJ), a region previously implicated in various aspects of social cognition, including suppression of egocentric biases (Silani et al., 2013), perspective taking (Saxe, 2006; Tusche et al., 2016), and pro-social behavior (Morishima et al., 2012; Hutcherson et al., 2015). However, the timing of this response, as well as the failure of time-varying egocentrically-biased computational models to better account for choice and RT patterns, are both inconsistent with the idea that such perspective-taking mechanisms activated slowly, *after* the emergence of a default self-centered bias (Epley et al., 2004; Tamir and Mitchell, 2013).

Nonetheless, we do find evidence for late-acting, response-related control mechanisms. We observed a comparatively late ERP signal differentiating choices by recipient from –300 ms before response. Whereas the stimulus-locked component showed an increased response specifically for the *Dissimilar* recipient, this neural activity predominantly distinguished the *Similar* condition. Yet, in contrast to the idea that this signal might be needed to correct or inhibit egocentric values, our computational analyses linked it only to variation in the response threshold for choice. What could be driving increases in response threshold for the similar recipient? One possible factor could be choice uncertainty. In line with this idea, participants took longer on average and had higher decision thresholds when choosing for the similar other, suggesting the need for additional evidence accumulation relative to the other conditions. Additionally, weights on taste were modestly but consistently lower for the similar other compared to choices for one's self, while weights on health were slightly higher, suggesting that participants may have "hedged" their choices where the similar other was concerned. These results provide a different perspective on the role of controlled processing in self-other decision-

making. They suggest that some forms of controlled processing may influence choices for others not by modifying value signals, but by raising the criterion for choice.

Given evidence of strong egocentric biases, rapid perspective-taking, and no computational evidence for delayed adjustment, what then explains patterns of longer response time when choosing differently from the self? Simulations performed using our combined neurocomputational model suggested that choices for self and other can diverge either due to differences in attribute weighting (as observed when making choices for the dissimilar other), or simply due to noise in the process of evidence accumulation (as observed when making choices for partners with similar preferences). In other words, trials where choices for self and similar others diverge may sometimes be trials on which choices for the self alone might be inconsistent from one instantiation to the next, due to ambivalent and noisy values. These will also tend to be the choices with the longest RTs, for both self and others. Although our model underestimated the observed RT differences somewhat, we suspect that the extra time may stem from conflict-triggered increases in threshold at the single-trial level (Cavanagh et al., 2011). This effect would tend to magnify the difference in RT beyond that predicted by a canonical DDM, in precisely those trials where divergent choices are most likely to be observed. Taken together, these results suggest that, at least in some decision scenarios, patterns of behavior previously associated with the action of both anchoring and adjustment may be better explained simply by anchoring, implemented in a stochastic decision system.

Note that these results do not argue against the basic idea of dual- or even multi-system models of choice. If anything, our results highlight the importance of *both* perspective-taking *and* response inhibition, and tie them to value integration and threshold computations, respectively. Moreover, there may be important decision scenarios in which choices for others do

engage dissociable correction or perspective-taking mechanisms, operating at different timescales (Epley et al., 2004; Evans, 2008). For example, our paradigm included no feedback. In cases where a decision maker must integrate both general information (e.g., knowledge about a person's culture, background, or similarity to oneself) and direct experience with another's choices, we might expect an initial egocentric preference that is corrected based on learning and memory (Devaine and Daunizeau, 2017; Tarantola et al., 2017). There may also be important individual differences in the speed or strength of social cognitive mechanisms, which might depend on the integrity of areas like the STS and TPJ. Our work highlights the utility of computational modeling for determining when patterns of choice, RT, and neural data that appear on their face to support dual-process models are instead more consistent with a single value integration mechanism (as observed in our study) and when additional computational mechanisms might be necessary to fully account for behavior.

Careful consideration of the timing of these processes also generates a novel prediction regarding the effects of time pressure versus cognitive load in social decision scenarios. Our data suggest that making accurate choices for people with divergent preferences relies more on early perspective-taking mechanisms, occurring from 300 to 500 ms post-stimulus onset in TPJ, while making accurate choices for partners with uncertain preferences relies more on later response threshold mechanisms localized to posterior cingulate cortex. If this is indeed the case, manipulations using time pressure or cognitive load may sometimes have quite different effects on social decision-making. Time pressure, which in perceptual choice has been tied to reductions in response threshold (Forstmann et al., 2010), might be expected to result in reduced accuracy only when others' preferences are uncertain. In contrast, cognitive load may disrupt effortful

perspective-taking mechanisms, resulting in stronger reductions in accuracy when preferences differ from the self.

Our work provides the first computational account of decision making capable of explaining the full pattern of choice, response times and neural dynamics when choosing for others, in a context where preferences are well-specified but can differ among individuals. Future studies will need to examine choices for others in different contexts and with different information. We believe that the unique combination of neural and computational modeling presented here provides a powerful and essential tool for this research, and will foster exciting new avenues for exploring how we choose for ourselves and others.

Author Contributions

A.H. and C.A.H. designed the experiment. A.H. collected the data. A.H., J.A.C., and C.A.H. analyzed the data. A.H., J.A.C., and C.A.H. interpreted the results and wrote the paper.

References

Andrews-Hanna JR, Reidler JS, Sepulcre J, Poulin R, Buckner RL (2010) Functional-anatomic fractionation of the brain's default network. Neuron 65:550-562.

Apps MA, Rushworth MF, Chang SW (2016) The Anterior Cingulate Gyrus and Social Cognition: Tracking the Motivation of Others. Neuron 90:692-707.

Bartra O, McGuire JT, Kable JW (2013) The valuation system: a coordinate-based meta-analysis of BOLD fMRI experiments examining neural correlates of subjective value. Neuroimage 76:412-427.

Belouchrani A, Abed-Meraim K, Cardoso J-F, Moulines E (1997) A blind source separation technique using second-order statistics. IEEE Transactions on Signal Processing 45:434-444.

Berkman ET, Hutcherson CA, Livingston JL, Kahn LE, Inzlicht M (2017) Self-Control as Value-Based Choice. Current directions in psychological science 26:422-428.

Cavanagh JF, Wiecki TV, Cohen MX, Figueroa CM, Samanta J, Sherman SJ, Frank MJ (2011) Subthalamic nucleus stimulation reverses mediofrontal influence over decision threshold. Nat Neurosci 14:1462-1467.

Clithero JA, Rangel A (2014) Informatic parcellation of the network involved in the computation of subjective value. Social cognitive and affective neuroscience 9:1289-1302.

Cohen MX, Cavanagh JF, Slagter HA (2011) Event-related potential activity in the basal ganglia differentiates rewards from nonrewards: temporospatial principal components analysis and source localization of the feedback negativity: commentary. Hum Brain Mapp 32:2270-2271.

1010 Crockett MJ (2016) How Formal Models Can Illuminate Mechanisms of Moral Judgment and
1011 Decision Making. Current directions in psychological science 25:85-90.
1012 Delorme A, Makeig S (2004) EEGLAB: an open source toolbox for analysis of single-trial EEG
1013 dynamics including independent component analysis. J Neurosci Methods 134:9-21.
1014 Delorme A, Sejnowski T, Makeig S (2007) Enhanced detection of artifacts in EEG data using
1015 higher-order statistics and independent component analysis. Neuroimage 34:1443-1449.
1016 Devaine M, Daunizeau J (2017) Learning about and from others' prudence, impatience or
1017 laziness: The computational bases of attitude alignment. PLoS Comput Biol
1018 13:e1005422.
1019 Epley N, Keysar B, Van Boven L, Gilovich T (2004) Perspective taking as egocentric anchoring
1020 and adjustment. J Pers Soc Psychol 87:327-339.
1021 Evans JSB (2008) Dual-processing accounts of reasoning, judgment, and social cognition. Annu
1022 Rev Psychol 59:255-278.
1023 Forstmann BU, Anwander A, Schafer A, Neumann J, Brown S, Wagenmakers EJ, Bogacz R,
1024 Turner R (2010) Cortico-striatal connections predict control over speed and accuracy in
1025 perceptual decision making. Proc Natl Acad Sci U S A 107:15916-15920.
1026 Friston K, Harrison L, Daunizeau J, Kiebel S, Phillips C, Trujillo-Barreto N, Henson R, Flandin
1027 G, Mattout J (2008) Multiple sparse priors for the M/EEG inverse problem. Neuroimage
1028 39:1104-1120.
1029 Gelman A, Rubin DB (1992) Inference from iterative simulation using multiple sequences.
1030 Statistical science:457-472.
1031 Grueschow M, Polania R, Hare TA, Ruff CC (2015) Automatic versus choice-dependent value
1032 representations in the human brain. Neuron 85:874-885.

1033 Hare TA, Camerer CF, Rangel A (2009) Self-control in decision-making involves modulation of
1034 the vmPFC valuation system. Science 324:646-648.
1035 Hare TA, Camerer CF, Knoepfle DT, Rangel A (2010) Value computations in ventral medial
1036 prefrontal cortex during charitable decision making incorporate input from regions
1037 involved in social cognition. J Neurosci 30:583-590.
1038 Hare TA, Schultz W, Camerer CF, O'Doherty JP, Rangel A (2011) Transformation of stimulus
1039 value signals into motor commands during simple choice. Proc Natl Acad Sci U S A
1040 108:18120-18125.
1041 Harris A, Lim SL (2016) Temporal Dynamics of Sensorimotor Networks in Effort-Based Cost-
1042 Benefit Valuation: Early Emergence and Late Net Value Integration. J Neurosci 36:7167-
1043 7183.
1044 Harris A, Hare T, Rangel A (2013) Temporally dissociable mechanisms of self-control: early
1045 attentional filtering versus late value modulation. J Neurosci 33:18917-18931.
1046 Harris A, Adolphs R, Camerer C, Rangel A (2011) Dynamic construction of stimulus values in
1047 the ventromedial prefrontal cortex. PLoS One 6:e21074.
1048 Henson RN, Mattout J, Singh KD, Barnes GR, Hillebrand A, Friston K (2007) Population-level
1049 inferences for distributed MEG source localization under multiple constraints: application
1050 to face-evoked fields. Neuroimage 38:422-438.
1051 Hunt LT, Kolling N, Soltani A, Woolrich MW, Rushworth MF, Behrens TE (2012) Mechanisms
1052 underlying cortical activity during value-guided choice. Nature neuroscience 15:470-476,
1053 S471-473.
1054 Hutcherson CA, Bushong B, Rangel A (2015) A Neurocomputational Model of Altruistic Choice
1055 and Its Implications. Neuron 87:451-462.

1056 Janowski V, Camerer C, Rangel A (2013) Empathic choice involves vmPFC value signals that
1057 are modulated by social processing implemented in IPL. Social cognitive and affective
1058 neuroscience 8:201-208.
1059 Jung TP, Makeig S, Humphries C, Lee TW, McKeown MJ, Iragui V, Sejnowski TJ (2000)
1060 Removing electroencephalographic artifacts by blind source separation.
1061 Psychophysiology 37:163-178.
1062 Krajbich I, Bartling B, Hare T, Fehr E (2015) Rethinking fast and slow based on a critique of
1063 reaction-time reverse inference. Nat Commun 6:7455.
1064 Kruschke JK (2013) Bayesian estimation supersedes the t test. J Exp Psychol Gen 142:573-603.
1065 Litt A, Plassmann H, Shiv B, Rangel A (2010) Dissociating Valuation and Saliency Signals
1066 during Decision-Making. Cereb Cortex.
1067 Litvak V, Friston K (2008) Electromagnetic source reconstruction for group studies. Neuroimage
1068 42:1490-1498.
1069 Morishima Y, Schunk D, Bruhin A, Ruff CC, Fehr E (2012) Linking brain structure and
1070 activation in temporoparietal junction to explain the neurobiology of human altruism.
1071 Neuron 75:73-79.
1072 Nicolle A, Klein-Flugge MC, Hunt LT, Vlaev I, Dolan RJ, Behrens TE (2012) An agent
1073 independent axis for executed and modeled choice in medial prefrontal cortex. Neuron
1074 75:1114-1121.
1075 Picton TW, Bentin S, Berg P, Donchin E, Hillyard SA, Johnson R, Jr., Miller GA, Ritter W,
1076 Ruchkin DS, Rugg MD, Taylor MJ (2000) Guidelines for using human event-related
1077 potentials to study cognition: recording standards and publication criteria.
1078 Psychophysiology 37:127-152.

1079 Plassmann H, O'Doherty J, Rangel A (2007) Orbitofrontal cortex encodes willingness to pay in
1080 everyday economic transactions. J Neurosci 27:9984-9988.
1081 Rangel A, Clithero J (2013) The computation of stimulus values in simple choice. In:
1082 Neuroeconomics: Decision Making and the Brain (Glimcher PW, Ferh E, eds): Academic
1083 Press.
1084 Ratcliff R, McKoon G (2008) The diffusion decision model: theory and data for two-choice
1085 decision tasks. Neural Comput 20:873-922.
1086 Ratcliff R, Smith PL, Brown SD, McKoon G (2016) Diffusion decision model: current issues
1087 and history. Trends in cognitive sciences 20:260-281.
1088 Ross L, Greene D, House P (1977) The "false consensus effect": An egocentric bias in social
1089 perception and attribution processes. Journal of experimental social psychology 13:279-
1090 301.
1091 Ruff CC, Fehr E (2014) The neurobiology of rewards and values in social decision making. Nat
1092 Rev Neurosci 15:549-562.
1093 Saxe R (2006) Uniquely human social cognition. Curr Opin Neurobiol 16:235-239.
1094 Silani G, Lamm C, Ruff CC, Singer T (2013) Right supramarginal gyrus is crucial to overcome
1095 emotional egocentricity bias in social judgments. J Neurosci 33:15466-15476.
1096 Smith PL, Ratcliff R (2004) Psychology and neurobiology of simple decisions. Trends Neurosci
1097 27:161-168.
1098 Spiegelhalter DJ, Best NG, Carlin BP, Van Der Linde A (2002) Bayesian measures of model
1099 complexity and fit. Journal of the Royal Statistical Society: Series B (Statistical
1100 Methodology) 64:583-639.

1101 Strait CE, Blanchard TC, Hayden BY (2014) Reward value comparison via mutual inhibition in
1102 ventromedial prefrontal cortex. Neuron 82:1357-1366.
1103 Strombach T, Weber B, Hangebrauk Z, Kenning P, Karipidis II, Tobler PN, Kalenscher T (2015)
1104 Social discounting involves modulation of neural value signals by temporoparietal
1105 junction. Proceedings of the National Academy of Sciences 112:1619-1624.
1106 Tamir DI, Mitchell JP (2010) Neural correlates of anchoring-and-adjustment during mentalizing.
1107 Proc Natl Acad Sci U S A 107:10827-10832.
1108 Tamir DI, Mitchell JP (2013) Anchoring and adjustment during social inferences. J Exp Psychol
1109 Gen 142:151-162.
1110 Tang AC, Sutherland MT, McKinney CJ (2005) Validation of SOBI components from high-
1111 density EEG. Neuroimage 25:539-553.
1112 Tarantola T, Kumaran D, Dayan P, De Martino B (2017) Prior preferences beneficially influence
1113 social and non-social learning. Nature Communications 8:817.
1114 Tusche A, Hutcherson CA (in press) Cognitive regulation alters social and dietary choice by
1115 changing attribute representations in domain-general and domain-specific brain circuits.
1116 eLife.
1117 Tusche A, Böckler A, Kanske P, Trautwein F-M, Singer T (2016) Decoding the charitable brain:
1118 empathy, perspective taking, and attention shifts differentially predict altruistic giving.
1119 Journal of Neuroscience 36:4719-4732.
1120 Uriguen JA, Garcia-Zapirain B (2015) EEG artifact removal-state-of-the-art and guidelines. J
1121 Neural Eng 12:031001.

1122 Volz LJ, Welborn BL, Gobel MS, Gazzaniga MS, Grafton ST (2017) Harm to self outweighs
1123 benefit to others in moral decision making. Proceedings of the National Academy of
1124 Sciences:201706693.
1125 Wiecki TV, Sofer I, Frank MJ (2013) HDDM: Hierarchical Bayesian estimation of the Drift-
1126 Diffusion Model in Python. Front Neuroinform 7:14.
1127

1128 **Figure Legends**

1129

1130 **Figure 1.** Social food choice task. (A) Experimental session. In Part 1, hungry participants with
1131 unrestricted diets were introduced to two partners, and provided taste and health ratings for the
1132 foods used in the experiment. Then, in Part 2, participants made food choices for themselves and
1133 the partners while their brain activity was measured with EEG. Participants knew that their
1134 choices mattered because a single trial was randomly selected and implemented for each
1135 recipient in Part 3. (B) Sample statements from the *Similar* (top) and *Dissimilar* (bottom)
1136 partners in the experiment. (C) Sample stimuli and screens from the decision task.

1137

1138 **Figure 2.** Behavioral results. (A) Percentage of healthy choices for each recipient. (B) Average
1139 observed RT by recipient. (C-E) Observed RT for trials separated on the basis of whether, given
1140 the same food option, the decision maker chose the same for (C) *Own* vs. *Similar*, (D) *Own* vs.
1141 *Dissimilar*, and (E) *Dissimilar* vs. *Similar*. Thus, *Own*-*Similar*:Same Response reflects RT for
1142 trials in which the choice was for *Own* self, and the response was the same as for the *Similar*
1143 other, whereas *Own*-*Similar*:Different Response reflects RTs on those trials where the response
1144 was different from the comparable choice for the *Similar* other; and likewise for the other
1145 comparisons.

1146

1147 **Figure 3.** ERP analysis of stimulus value integration by recipient. (A) Heat map of significant *P*
1148 values associated with stimulus value, showing significant effects from 500 to 650 ms (green
1149 box) and 700 to 850 ms (blue box) after stimulus onset. (B) Source reconstructions from 500 to
1150 650 ms (green) and 700 to 850 ms (blue) overlaid on a representative brain image. Particularly

during the earlier 500-650 ms window, stimulus value activity was localized to regions including VMPFC (circled). Inset, top: Spherical masks based on peak coordinates from three neuroimaging studies [blue (Plassmann et al., 2007), magenta (Hare et al., 2009), cyan (Litt et al., 2010)]. Inset, bottom: Source localization of stimulus value from approximately 450 to 600 ms post-stimulus onset in two ERP studies [red: (Harris et al., 2013), yellow: (Harris and Lim, 2016)]. (C) Stimulus value integration by recipient. Topographic scalp distribution (left) and average waveforms for the linear ordering of stimulus value (red: Strong No; orange: Weak No; cyan: Weak Yes; green: Strong Yes) in the 500-650 ms window (shaded green box) and 700-850 ms window (shaded blue box), plotted separately for each recipient (*Own*: solid, *Similar*: dashed; *Dissimilar*: dotted). (D) Comparison of scalp topography from 800 to 850 ms post-stimulus for the main effect of stimulus value (top), the interaction of stimulus value with *Similar* recipient (middle) and the interaction of stimulus value with *Dissimilar* recipient (bottom) revealed significant reductions in stimulus value signals for the two other recipients during the late window, in line with average waveform data in (C).

Figure 4. ERP analysis of attribute weighting by recipient. (A) Scalp topography during *a priori* time window of interest from 500 to 650 ms post-stimulus revealed differences in neural weighting of taste ratings (left) and health ratings (middle) by recipient. Sensors of interest (SOI) were identified by taking the conjunction of sensors showing significant ERP activity for *Similar* and *Dissimilar* in the Taste – Health comparison (black box, right). (B) Average waveforms associated with the linear ordering of taste (left) and health (right) plotted separately for each recipient (*Own*: solid; *Similar*: dashed; *Dissimilar*: dotted). Orange: taste; Green: health. (C-D) Linear contrast weights for taste (C) and health (D) as a function of recipient.

Figure 5. Differences in average ERP waveforms by recipient identity. (A) Heat map of significant *P* values showing stimulus-locked regression results for the main effects of *Similar* (left) and *Dissimilar* (right). Significant effects were visible for the *Dissimilar* recipient, but not the *Similar* recipient, at time windows including 350 to 400 ms after stimulus onset (green box). (B) Scalp topography (left) and average waveforms (right) associated with choice recipient identity (*Own* self: cyan, *Similar* other: blue, *Dissimilar* other: orange) 350-400 ms post-stimulus onset. Inset: Source reconstruction from 350-400 ms post-stimulus overlaid on a representative brain image localized this response to regions including the temporoparietal junction (TPJ) and superior temporal sulcus (STS). (C). Heat map of significant *P* values showing response-locked regression results for the main effects of *Similar* (left) and *Dissimilar* (right). Significant effects were visible for the *Similar* recipient, but not *Dissimilar* recipient, approximately 300ms to 180 ms prior to the response (green box). Later effects in the Dissimilar condition coincide with motor activity related to initiation of the key press response. (D) Scalp topography (left) and average waveforms (right) associated with choice recipient identity (*Own* self: cyan, *Similar* other: blue, *Dissimilar* other: orange). Inset: Source reconstruction from 300 to 180 ms prior to the response localized this differential response to regions including the intraparietal sulcus (IPS).

Figure 6. Hierarchical Bayesian parameter estimates of the influence of neural response on model parameters. (A-C) Trial-by-trial fluctuations in the ERP in sensors-of-interest (SOIs) for the value-related ERP from 500-650ms (A) were linked with significantly greater influence on the drift rate *v* of the taste attribute when choosing for *Own* self and *Similar* other (B) and the

health attribute when choosing for the *Dissimilar* other (C), suggesting that this response relates to evidence accumulation in the computational model. (D-F) Trial-by-trial fluctuations in the response-locked ERP component (D) differentiated choices for the *Similar* other to a greater extent than *Dissimilar* or *Own* choices, consistent with computational model-fitting of the behavioral barrier parameter (E), and likewise demonstrated a significant influence on the barrier for response (F).

Figure 7. DDM simulations. (A) Simulations (N=10000) of RT data for same versus different choice using best-fitting specification M2. Trials are separated based on the same criteria described for observed data in Figure 2, with observed data (left) plotted next to predicted model RTs (right) for each combination of recipient. (B-C) Predicted (B) and observed (C) relationship between drift rates and percentage of different choices when comparing choices for two recipients, simulated separately for each of the 16 possible combinations of health and taste rating. Proximity of the dots to the diagonal reflects similarity of food values for two recipients, and size and color of dots are coded according to the percentage of different choices. Additional details are provided in the main text.

Table 1: DDM Specifications Summary

Parameter w/ Trialtype	Model#	DIC	MSE Choice	MSE RT Yes	MSE RT No
v	M1	46384.2	0.0137	0.0537	0.0694
v,a	M2	46318.6	0.0135	0.0532	0.0689
v,z	M3	46522.1	0.0137	0.0559	0.0655
v,a,z	M4	46415.6	0.0137	0.0538	0.0682

Note: v = drift rate, a = threshold, z = starting point.

Table 2: DDM posterior estimates and convergence for Model M2

Parameter	**Mean**	**Stdev**
Drift (v), Intercept	-1.982	0.055
Drift (v), HealthOwn	0.062	0.011
Drift (v), HealthSimilar	0.183	0.010
Drift (v), HealthDissimilar	0.660	0.011
Drift (v), TasteOwn	0.722	0.011
Drift (v), TasteSimilar	0.665	0.010
Drift (v), TasteDissimilar	0.007	0.011
Barrier (a), Intercept	2.006	0.047
Barrier (a), Similar	0.125	0.015
Barrier (a), Dissimilar	0.049	0.015
Starting point (z)	0.493	0.006
NonDecisionTime	0.357	0.026
Convergence	**Mean**	**Stdev**
$\hat{R}$	1.0002	0.0002

Note: Statistics for parameter estimates reflect the mean and standard deviation of the N=10000 posterior samples of group-level parameters.

A

I. Set-Up	II. EEG	III. Outcome
• *Photo taken* • *Partner introductions* • *Taste/Health ratings*	*Decision (6 runs) for:* • *Own Self* • *Similar Partner* • *Dissimilar Partner*	*Receive random food based on decision*

B

Similar: No dietary restrictions

Dissimilar: Self-identified healthy eater

C

Sample Trial, Decision Task

Until response (max 4 s)

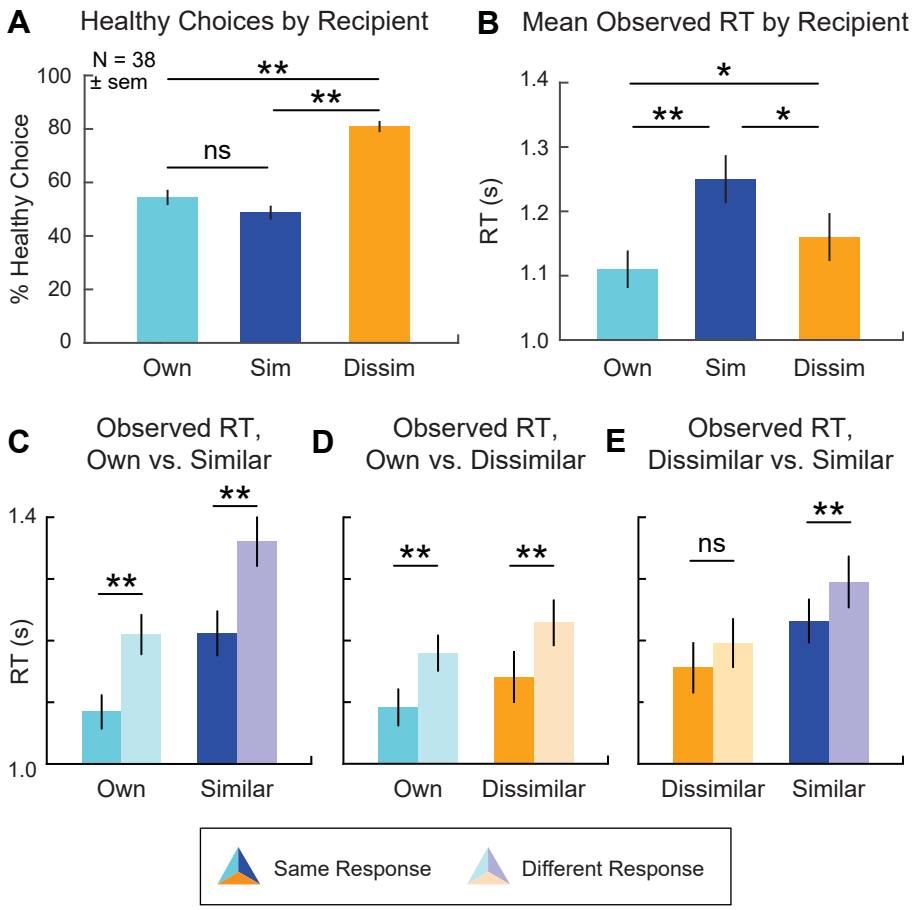
A
Healthy Choices by Recipient
N = 38
± sem
% Healthy Choice
100
80
60
40
20
0
**
**
ns
Own
Sim
Dissim
B
Mean Observed RT by Recipient
RT (s)
1.4
1.3
1.2
1.1
1.0
*
**
*
Own
Sim
Dissim
C
Observed RT,
Own vs. Similar
RT (s)
1.4
1.0
**
**
Own
Similar
D
Observed RT,
Own vs. Dissimilar
**
**
Own
Dissimilar
E
Observed RT,
Dissimilar vs. Similar
ns
**
Dissimilar
Similar
Same Response
Different Response

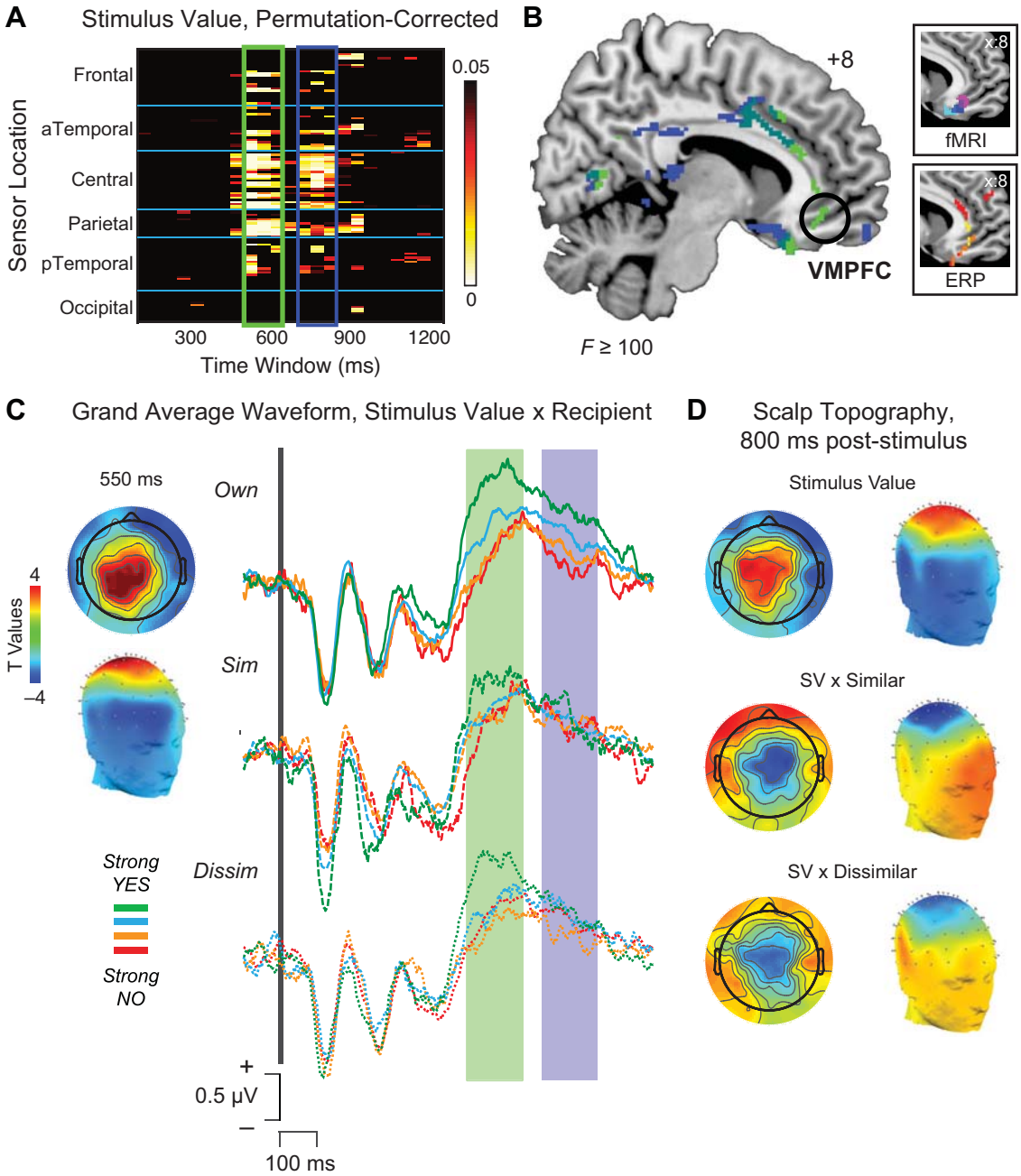
A
Stimulus Value, Permutation-Corrected
Sensor Location
Frontal
aTemporal
Central
Parietal
pTemporal
Occipital
0.05
0
300
600
900
1200
Time Window (ms)
B
+8
VMPFC
F ≥ 100
x:8
fMRI
x:8
ERP
C
Grand Average Waveform, Stimulus Value x Recipient
550 ms
T Values
4
–4
Own
Sim
Dissim
Strong YES
Strong NO
+
0.5 μV
–
100 ms
D
Scalp Topography, 800 ms post-stimulus
Stimulus Value
SV x Similar
SV x Dissimilar

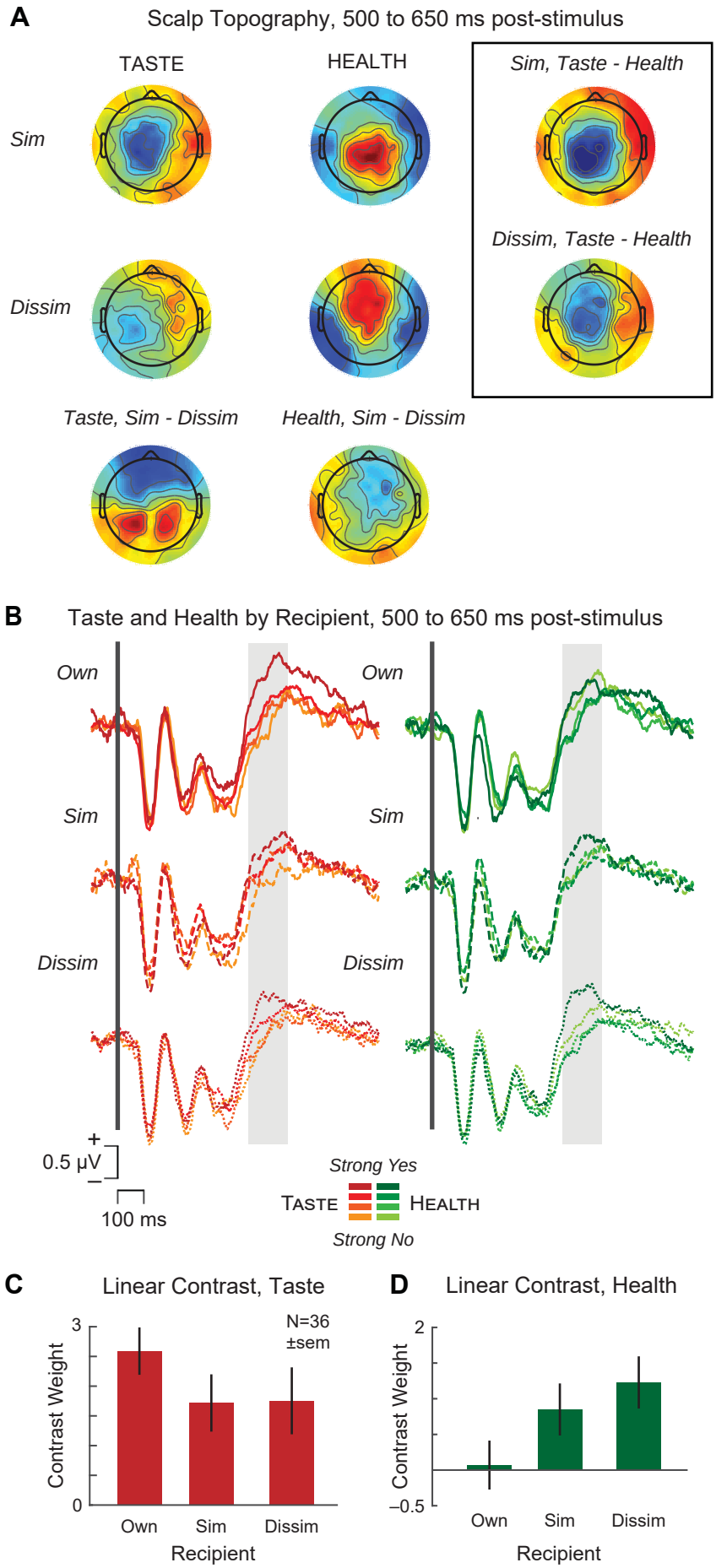
A
Scalp Topography, 500 to 650 ms post-stimulus
TASTE
HEALTH
Sim, Taste - Health
Sim
Dissim
Dissim, Taste - Health
Taste, Sim - Dissim
Health, Sim - Dissim
B
Taste and Health by Recipient, 500 to 650 ms post-stimulus
Own
Sim
Dissim
Own
Sim
Dissim
+
0.5 µV
–
100 ms
Strong Yes
TASTE
HEALTH
Strong No
C
Linear Contrast, Taste
N=36
±sem
Contrast Weight
3
0
Own
Sim
Dissim
Recipient
D
Linear Contrast, Health
Contrast Weight
2
–0.5
Own
Sim
Dissim
Recipient

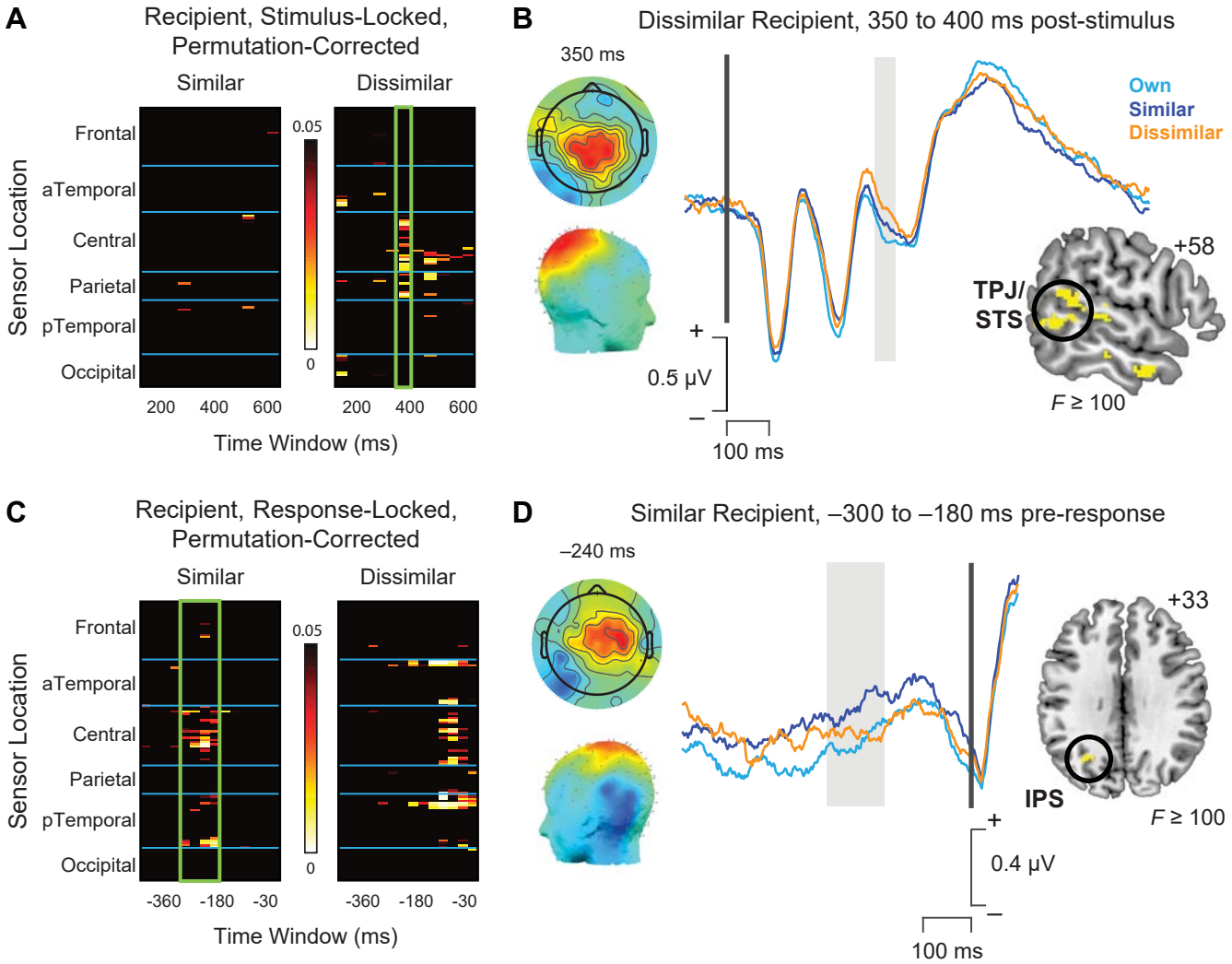
A
Recipient, Stimulus-Locked, Permutation-Corrected
Similar
Dissimilar
Sensor Location
Frontal
aTemporal
Central
Parietal
pTemporal
Occipital
0.05
0
200
400
600
Time Window (ms)
B
Dissimilar Recipient, 350 to 400 ms post-stimulus
350 ms
Own
Similar
Dissimilar
+
0.5 μV
–
100 ms
+58
TPJ/
STS
F ≥ 100
C
Recipient, Response-Locked, Permutation-Corrected
Similar
Dissimilar
Sensor Location
Frontal
aTemporal
Central
Parietal
pTemporal
Occipital
0.05
0
-360
-180
-30
Time Window (ms)
D
Similar Recipient, –300 to –180 ms pre-response
–240 ms
+33
IPS
F ≥ 100
+
0.4 μV
–
100 ms

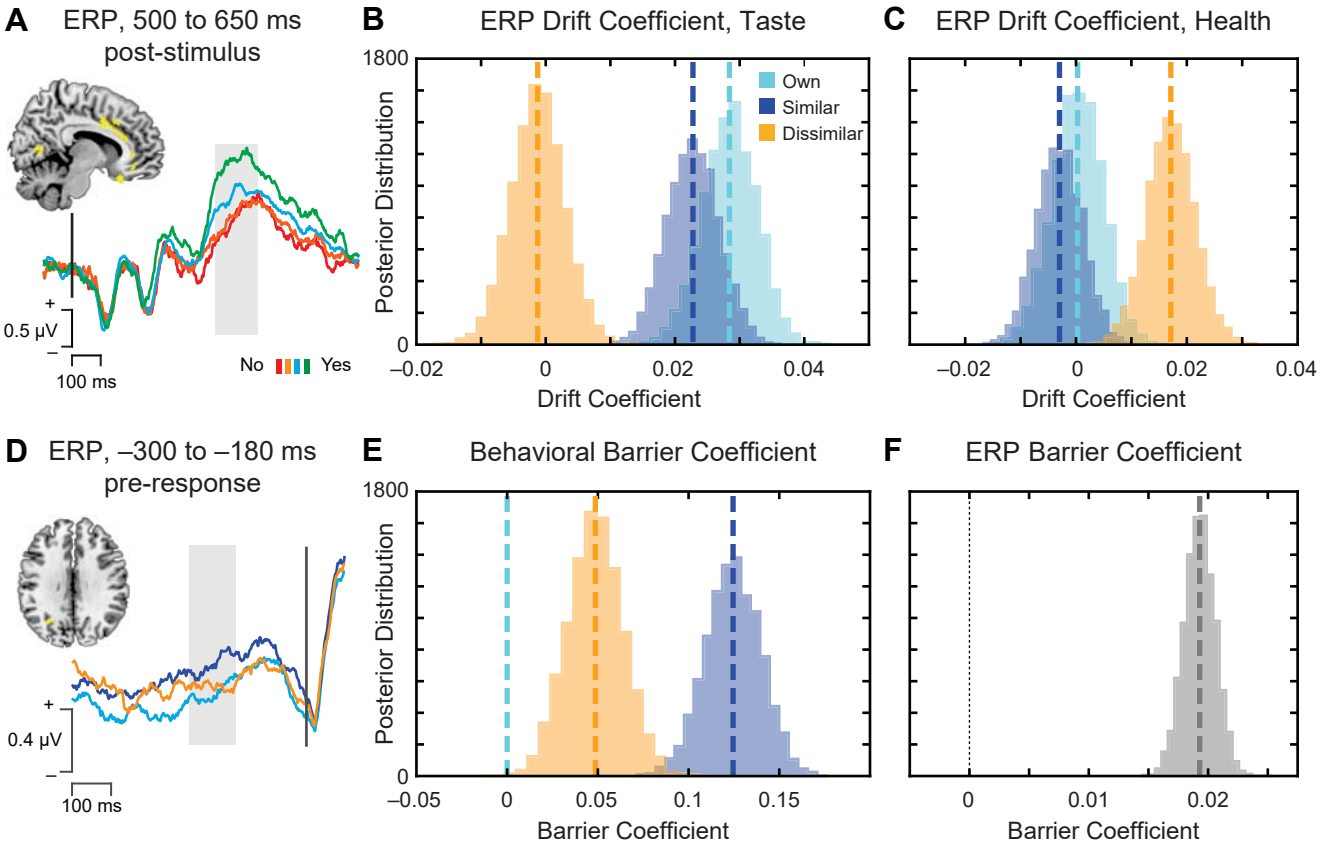
A
ERP, 500 to 650 ms post-stimulus
0.5 μV
100 ms
No
Yes
B
ERP Drift Coefficient, Taste
1800
0
Posterior Distribution
Own
Similar
Dissimilar
–0.02
0
0.02
0.04
Drift Coefficient
C
ERP Drift Coefficient, Health
–0.02
0
0.02
0.04
Drift Coefficient
D
ERP, –300 to –180 ms pre-response
0.4 μV
100 ms
E
Behavioral Barrier Coefficient
1800
0
Posterior Distribution
–0.05
0
0.05
0.1
0.15
Barrier Coefficient
F
ERP Barrier Coefficient
0
0.01
0.02
Barrier Coefficient

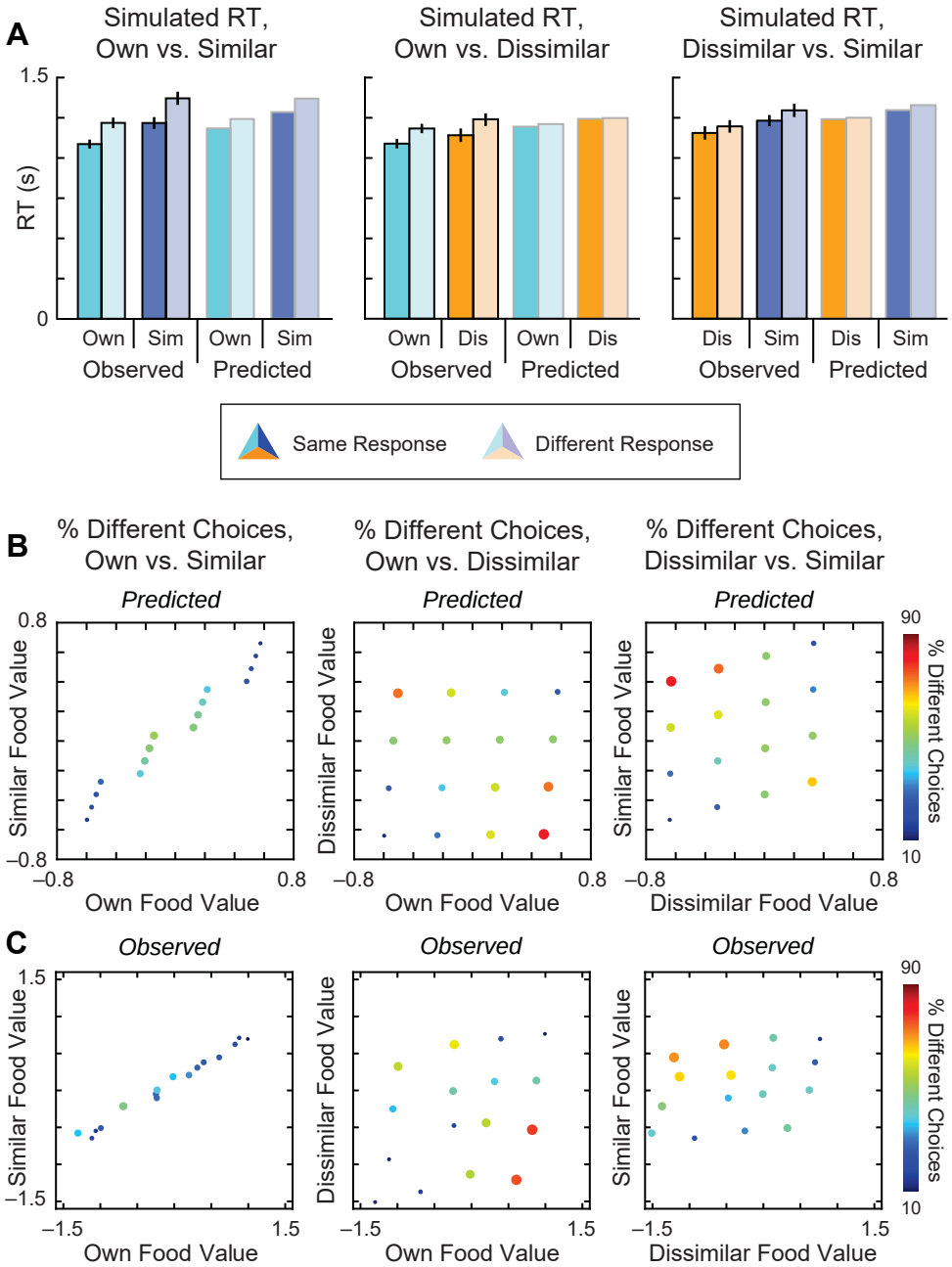
A
Simulated RT, Own vs. Similar
Simulated RT, Own vs. Dissimilar
Simulated RT, Dissimilar vs. Similar
RT (s)
1.5
0
Own
Sim
Dis
Observed
Predicted
Same Response
Different Response
B
% Different Choices, Own vs. Similar
% Different Choices, Own vs. Dissimilar
% Different Choices, Dissimilar vs. Similar
Predicted
Similar Food Value
Dissimilar Food Value
Own Food Value
0.8
–0.8
% Different Choices
90
10
C
Observed
1.5
–1.5